Bioconjugate Chemistry

Article

pubs.acs.org/bc

Design and Synthesis of Amphiphilic and Luminescent Tris-Cyclometalated Iridium(III) Complexes Containing Cationic Peptides as Inducers and Detectors of Cell Death via a Calcium-Dependent Pathway

Yosuke Hisamatsu,[†] Ai Shibuya,[†] Nozomi Suzuki,[†] Toshihiro Suzuki,[‡] Ryo Abe,[‡] and Shin Aoki*[,†,§]

[†]Faculty of Pharmaceutical Sciences, [‡]Research Institute for Biomedical Sciences, and [§]Division of Medical Science-Engineering Corporation, Research Institute of Science and Technology, Tokyo University of Science, 2641 Yamazaki, Noda, Chiba 278-8510, Japan

Supporting Information

ABSTRACT: Cationic amphiphilic peptides have the potential to function as agents for the treatment of microbial infections and cancer therapy. The cationic and hydrophobic parts of these molecules allow them to associate strongly with negatively charged bacterial or cancer cell membranes, thus exerting antimicrobial and anticancer activities through membrane disruption. Meanwhile, cyclometalated iridium(III) complexes such as *fac*-Ir(ppy)$_3$ (ppy = 2-phenylpyridine) and *fac*-Ir(tpy)$_3$ (tpy = 2-(4′-tolyl)pyridine) possess C_3-symmetric structures and excellent photophysical properties as phosphorescence materials, which make them important candidates for use in biological applications such as chemosensors, biolabeling, living cell staining, in vivo tumor imaging, and anticancer agents. We recently reported on some regioselective substitution reactions of Ir(tpy)$_3$ and Ir(ppy)$_3$ at the 5′-position (*p*-position with respect to the C−Ir bond) on the 2-phenylpyridine ligands and their subsequent conversions to a variety of functional groups. We report here on the design and synthesis of amphiphilic and luminescent tris-cyclometalated Ir complexes in which cationic peptides are attached through alkyl chain linkers that work as inducers and detectors of cell death. Ir complexes containing cationic peptides such as a KKGG sequence and alkyl chain linkers of adequate length (C6 and C8) exhibit considerable cytotoxicity against cancer cells such as Jurkat, Molt-4, HeLa-S3, and A549 cells, and that dead cells are well stained with these Ir complexes. Furthermore, an Ir complex in which the KKGG peptide is attached through a C6 linker displayed lower cytotoxicity against normal mouse lymphocytes. Mechanistic studies suggest that Ir complexes containing the KKGG peptide interact with anionic molecules on the cell surface and/or membrane receptors to trigger the Ca^{2+} dependent pathway and intracellular Ca^{2+} response, resulting in necrosis accompanied by membrane disruption.

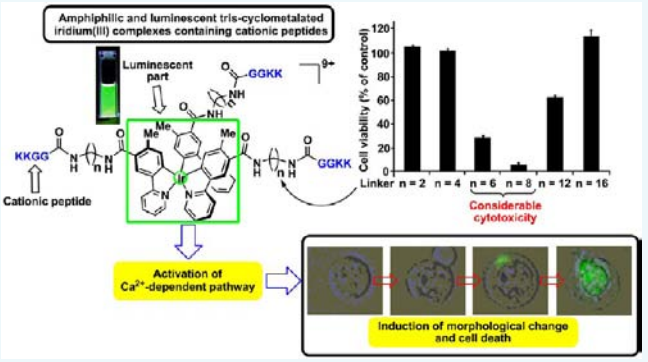

INTRODUCTION

Cationic amphiphilic peptides (CAPs) have received considerable attention as reagents for nonviral gene delivery,[1] the treatment of microbial infections,[2] cancer therapy,[3] and so on. Numerous studies support the conclusion that the electrostatic and hydrophobic properties of CAPs and their secondary structures such as α-helical or β-sheet structures play important roles in their association with negatively charged bacterial or cancer cell membranes, leading to their antimicrobial[2] and anticancer activity.[3]

It is known that cancer cell membranes have a net negative charge due to the elevated expression of anionic molecules such as phosphatidylserine, sialylated gangliosides, *O*-glycosylated mucins, and heparan sulfate.[3,4] In contrast, the surface of a normal cell is mainly composed of neutral zwitterionic phospholipid and sterols. Therefore, negatively charged cancer cell membranes represent a potential target for agents that have selective cytotoxicity against cancer cells.[3d,e,i] Namely, specific interactions with cancer cell membranes may result in fewer toxic side effects than are observed in cases of commonly used antineoplastic drugs.[3d,l] For instance, Schneider and co-workers reported that the anticancer peptide SVS-1 forms a cationic amphiphilic β-sheet structure on the cancer cell surface and exhibits higher cytotoxic activity against a variety of cancer cells than those of normal cells and erythrocytes.[3j,k] Stupp and co-workers recently reported that cell death or cell survival is affected by the supramolecular cohesion of nanostructures formed by self-assembled CAPs.[5] However, the relationships between structure and cytotoxicity and the details of the

Received: February 13, 2015
Revised: April 14, 2015
Published: April 15, 2015

DOI: 10.1021/acs.bioconjchem.5b00095
Bioconjugate Chem. 2015, 26, 857−879

mechanism by which amphiphiles induce cell death are not fully understood.

Meanwhile, cyclometalated iridium(III) complexes such as *fac*-Ir(ppy)$_3$ **1** (ppy = 2-phenylpyridine) and *fac*-Ir(tpy)$_3$ **2** (tpy = 2-(4′-tolyl)pyridine) have C_3-symmetric structures and excellent photophysical properties as phosphorescence materials (Chart 1).[6] They exhibit high photostabilities, larger Stokes' shifts, high phosphorescent quantum yields, and relatively longer lifetimes ($\tau \sim \mu s$) than those of many fluorescent molecules ($\tau \sim$ ns).[6] These attractive photochemical and structural properties make cyclometalated Ir complexes important candidates for use in biological applications such as chemosensors,[7] biolabeling,[8] living cell staining,[9] in vivo tumor imaging,[10] and anticancer agents.[11] Therefore, water-soluble peptide−Ir complex conjugates are considered to be promising candidates for biological and biomedicinal applications such as receptor-targeting cancer imaging, cancer therapy, and cell penetrating reagents, as well as related uses. However, examples of such Ir complexes are quite limited.[12,13]

We recently reported on some regioselective substitution reactions of **1** and **2** at the 5′-position (the *p*-position with respect to the C−Ir bond) on 2-phenylpyridine ligands and their subsequent conversions to produce **3** with a variety of functional groups (Chart 1).[14] For example, cellular imaging of pH-responsive Ir complexes containing diethyl amino groups[14c] or pyridyl groups[14d] at the 5′-position and their activities related to photoinduced cell death have been reported. It is assumed that these functionalization reactions would be a particularly powerful method for synthesis of a variety of Ir complexes possessing labile functional groups such as peptides, oligosaccharides, as well as other moieties that would otherwise be difficult to produce.

In this manuscript, we report on the design and synthesis of cationic amphiphilic Ir complexes as inducers and detectors of cell death. The complexes are composed of C_3-symmetric, hydrophobic, and luminescent tris-cyclometalated Ir scaffold with cationic peptides attached through alkyl linkers, as shown in Chart 2, and a determination of their cytotoxic activities against cancer cells and normal mouse lymphocytes was performed. The findings show that Ir complexes possessing KKGG sequences (K: lysine, G: glycine) linked by alkyl chain linkers with a suitable length exhibit a considerable cytotoxicity against cancer cells such as Jurkat, Molt-4, HeLa-S3, and A549 cells. For comparison, the trispeptide having a benzene-1,3,5-tricarboxamide core **10**[15] and the dansyl-containing peptide **11** were synthesized. Structure−cytotoxicity relationships, mecha-

Chart 1

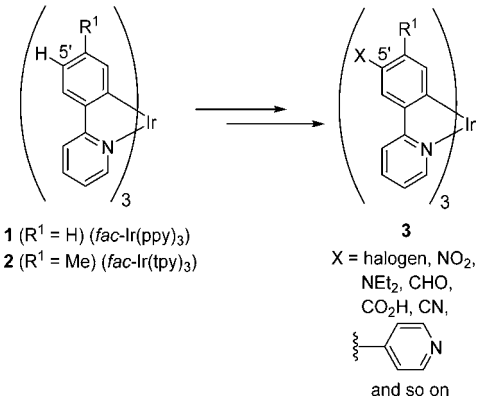

Chart 2

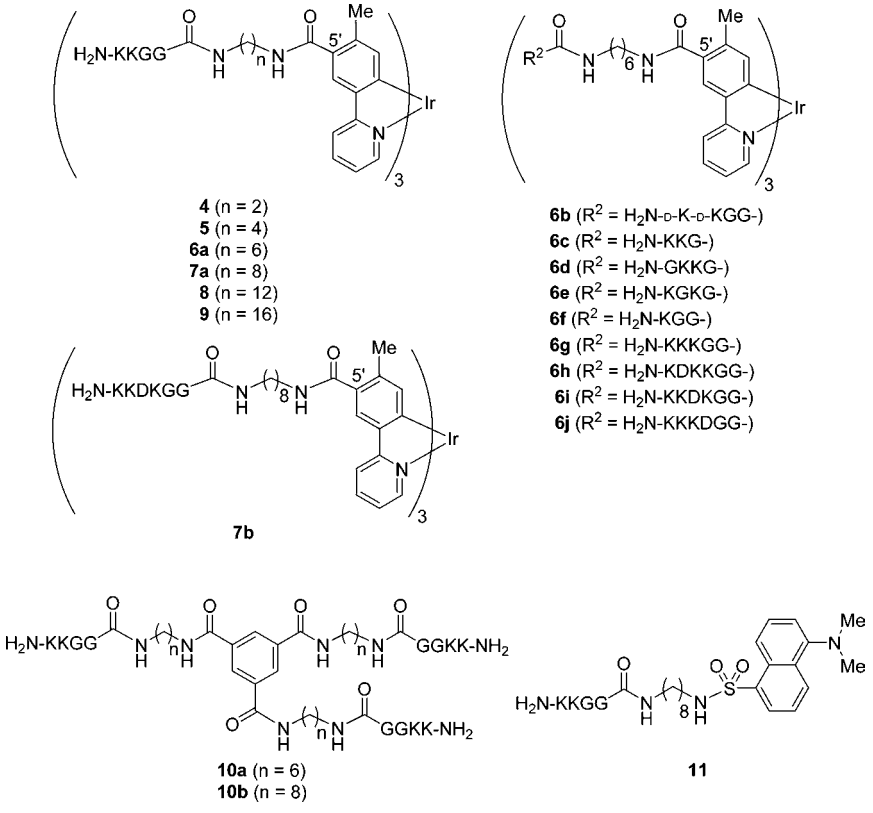

DOI: 10.1021/acs.bioconjchem.5b00095
Bioconjugate Chem. 2015, 26, 857−879

Chart 3

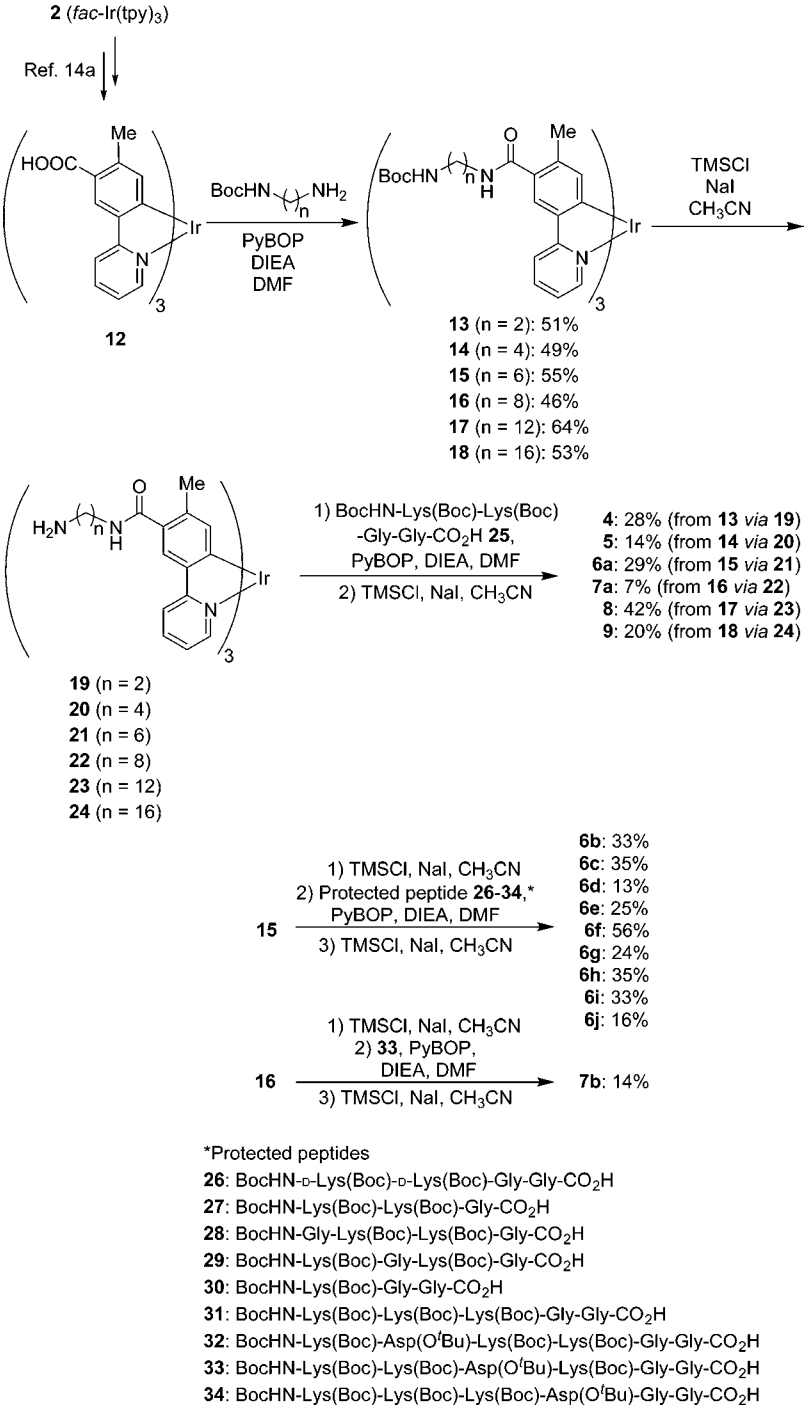

nistic studies of the Ir complexes based on the direct observation of their luminescent imaging, are reported.

RESULTS AND DISCUSSION

Design and Synthesis of Amphiphilic Ir Complexes with an Attached Cationic Peptide. The synthesis of amphiphilic Ir complexes having basic peptides is shown in Chart 3. The central Ir unit **12** was synthesized from **2** (as a racemic mixture of Δ and Λ forms), as described in a previous report.[14a] The condensation of **12** with a mono-Boc-protected diamine derivative gave **13**−**18** (n = 2, 4, 6, 8, 12, 16), Boc groups of which were removed by treatment with TMSCl and NaI to give **19**−**24**.[16] The protected KKGG peptide **25** prepared by Fmoc solid-phase peptide synthesis was coupled with **19**−**24** to give Ir complexes containing the corresponding fully protected peptides. We first attempted to remove the protecting groups from the peptides on the Ir complexes with a TFA cocktail (TFA/H_2O/^{i}Pr_3SiH), but this procedure resulted in decomposition of the Ir complex core under the strong acidic conditions. Therefore, the deprotection was performed by treatment with TMSCl and NaI in CH_3CN[14a,16] and the resulting products were purified by RP-HPLC to give the TFA salts of **4**, **5**, **6a**, **7a**, **8**, and **9** as yellow solids. Other Ir complexes having peptides were synthesized similarly. It should

DOI: 10.1021/acs.bioconjchem.5b00095
Bioconjugate Chem. 2015, 26, 857−879

be noted that diastereomers of these Ir complexes resulting from the racemic Ir complex center were not distinguished in ^{1}H NMR spectra and hence were not separated in this work. The benzene-1,3,5-tricarboxamide derivatives **10a** and **10b**, and the dansylamide derivative **11** containing a KKGG peptide monomer, were also prepared as reference compounds (Chart S2 in Supporting Information).

Photophysical Properties of Ir Complexes. UV−vis and luminescent spectra of representative Ir complexes, **5**, **6a**, **7a**, **8**, and **9** (10 μM) in degassed 100 mM HEPES at pH 7.4 and 25 °C are shown in Figure 1 and their photophysical data are

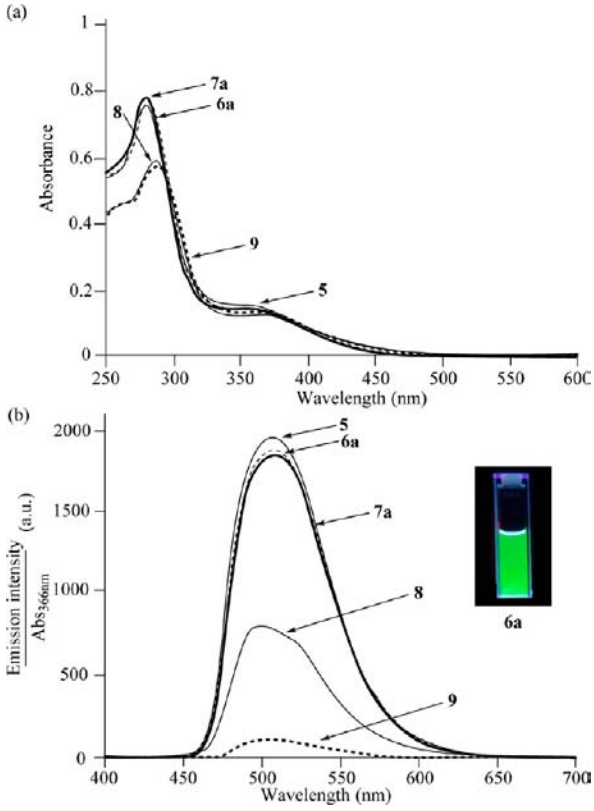

Figure 1. (a) Absorption and (b) emission spectra of **5** (solid curve), **6a** (dashed curve), **7a** (bold curve), **8** (solid curve), and **9** (bold dashed curve) in degassed 100 mM HEPES (pH 7.4) at 25 °C ([Ir complex] = 10 μM, excitation at 366 nm). a.u. is arbitrary unit. (Inset) Photograph showing emission of **6a** (excitation at 365 nm).

summarized in Table 1. The concentrations of these Ir complexes in stock solutions (PBS: phosphate buffer saline)

Table 1. Photophysical Properties of Ir Complexes, 2, 5, 6a, 7a, 8, and 9[a]

compound	λ_{max} (absorption)	λ_{max} (emission)	Φ[c]	τ
2[b] (in CH_2Cl_2)	287 nm, 373 nm	512 nm	0.50	2.0 μs[d]
5	280 nm, 359 nm	508 nm	0.57	1.7 μs
6a	280 nm, 362 nm	509 nm	0.55	1.7 μs
7a	280 nm, 358 nm	509 nm	0.54	1.3 μs
8	284 nm, 370 nm	499 nm	0.19	1.2 μs
9	286 nm, 361 nm	502 nm	0.03	0.46 μs

[a]([Ir complex] = 10 μM, excitation at 366 nm) in degassed CH_2Cl_2 or 100 mM HEPES (pH 7.4) at 25 °C. [b]Ref 14a. [c]Quinine sulfate in 0.1 M H_2SO_4 (Φ = 0.55) were used as a reference. [d]Ref 6b.

are determined from the molar extinction coefficient at 380 nm ($\varepsilon_{380\ nm}$ = (1.08 ± 0.07) × 10^4 M^{-1} cm^{-1}) of **19** and **21** that are characterized by elemental analysis. The UV−vis spectra of **5**, **6a**, and **7a** were nearly identical to those of typical Ir(tpy)$_3$ derivatives in CH_2Cl_2 (Figure 1a).[6e,17] The strong absorption bands ca. 280 nm were assigned to the $^1\pi-\pi^*$ transition of the tpy ligands and the weak shoulder bands at ca. 350−500 nm can be assigned spin-allowed singlet-to-singlet metal-to ligand charge transfer (^{1}MLCT) transitions, spin-forbidden singlet-to-triplet (^{3}MLCT) transitions, and $^3\pi-\pi^*$ transitions. In luminescent spectra, a green emission was observed from **5**, **6a**, **7a**, **8**, and **9** with emission maxima at ca. 506 nm (Figure 1b) and the luminescent quantum yields (Φ) of **5**, **6a**, and **7a** were determined to be 0.57, 0.55, and 0.54, respectively, and their luminescence lifetimes are in the range of 1.3−1.7 μs, similar to that for **2**[6b,e] (Table 1). On the other hand, the absorbances of **8** and **9** at ca. 280 nm corresponding to the $^1\pi-\pi^*$ transition state were decreased with a small red shift, with Φ values of 0.19 and 0.03, respectively.[17] The radiative and nonradiative rate constants, k_r and k_{nr}, of some Ir complexes in aqueous solutions are shown in Table S1 in Supporting Information, indicating that **8** and **9** have smaller K_r and greater K_{nr} values than those of **5**, **6a**, and **7a**. The relatively small Φ values of **8** and **9** can be attributed to radiationless deactivation due to the C12 and C16 alkyl chains and/or formation of small size self-assembly in aqueous solution.[17,18]

Cytotoxic Activity of Ir Complexes Containing Basic Peptides against Jurkat Cells Evaluated by Cell Imaging and MTT Assay. The cytotoxic activity of amphiphilic Ir complexes containing KKGG peptides against T-lymphocyte leukemia Jurkat cells was evaluated. Jurkat cells were incubated in 10% FCS (fetal calf serum) RPMI 1640 medium containing Ir(tpy)$_3$ **2**, **4** (n = 2), **5** (n = 4), **6a** (n = 6), **7a** (n = 8), **8** (n = 12), and **9** (n = 16) (50 or 75 μM) for 1 h at 37 °C under 5% CO_2, collected by centrifugation and washed with PBS containing 0.5% FCS and 0.1% NaN_3, and observed by fluorescent microscopy (Biorevo, BZ-9000, Keyence).

As shown in Figure 2a−c, Ir(tpy)$_3$ **2** (50 μM) moved into the cells at 37 °C, as evidenced by its green emission. On the other hand, cells incubated with **4** and **5** (75 μM) exhibited a normal morphology and the emission was negligible (Figure 2d−i). In the presence of **6a** and **7a** (50 μM), apparent morphological changes, possibly due to cell death (Figure 2j,m) and a strong green emission (exposure time: ca. 0.02 s) were observed in the dead cells (Figure 2k,l,n,o) (These phenomena are discussed below.[19]) Interestingly, **8** (50 μM) and **9** (50 μM) caused minimal cell death under the same conditions and their green emission was mainly observed on the cell membrane, indicating that **8** and **9** interacted with the negatively charged cell membrane (Figure 2p−u) without any apparent morphological change. It should be noted that the treatment of **6a** (50 μM) at 4 °C (on ice) for 1 h induced a negligible morphological change in Jurkat cells and **6a** was mainly located on the cell membrane (emission image was taken using a longer exposure time (0.25 s)), suggesting that **6a** initially interacted with the cell surface (Figure 2v−x). These behaviors provide good contrast with data for our previous Ir complexes, **35** and **36** (Chart 4), which are passively transported into the cells even at 4 °C and require photoirradiation to induce necrosis-like cell death.[14c,d]

The viability of Jurkat cells at increasing concentrations (0−50 μM) of Ir complexes **4**, **5**, **6a**, **7a**, **8**, and **9** was measured by means of MTT assay (MTT = 3-(4,5-dimethyl-2-thiazolyl)-2,5-

DOI: 10.1021/acs.bioconjchem.5b00095
Bioconjugate Chem. 2015, 26, 857−879

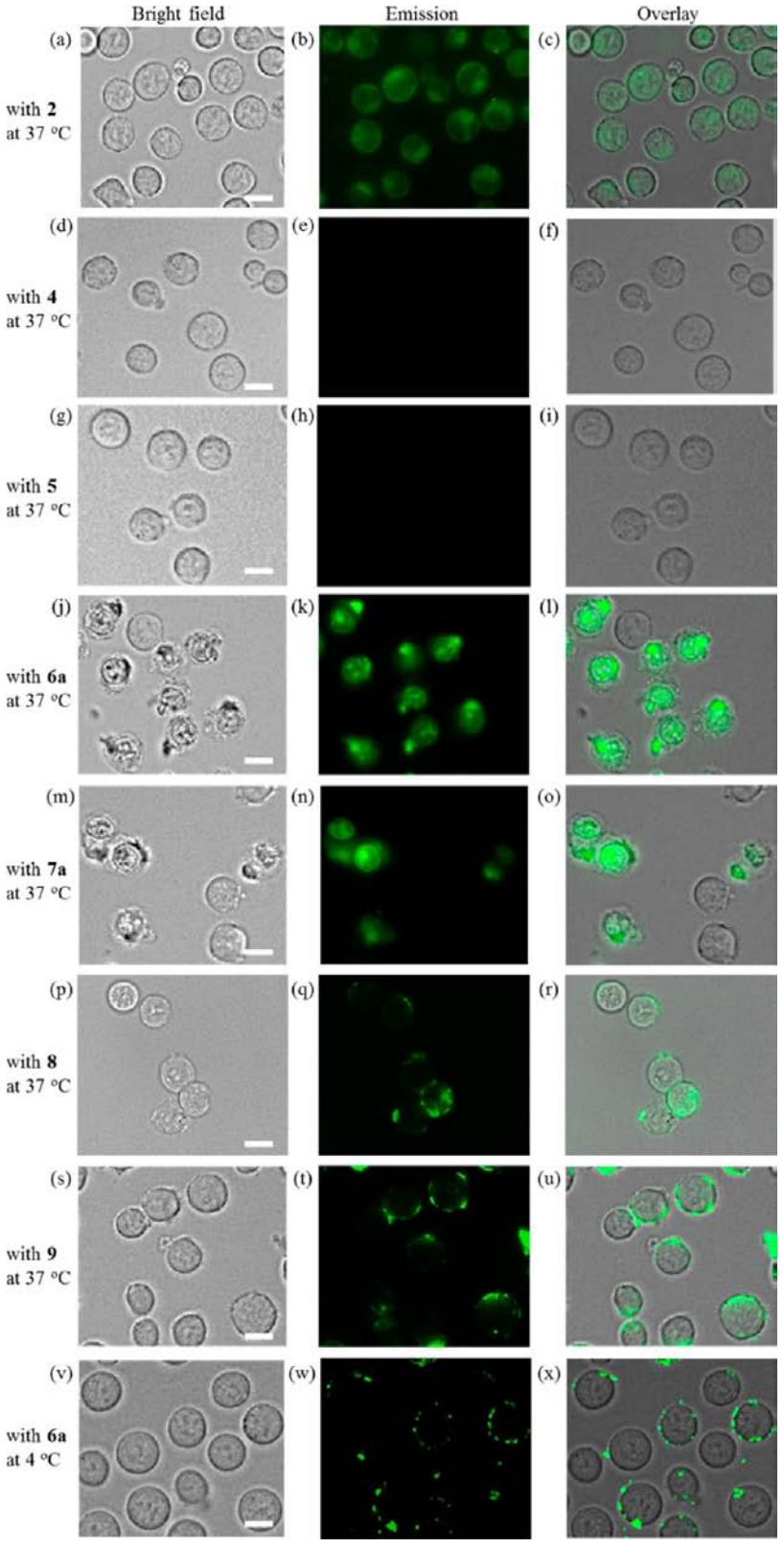

Figure 2. Typical luminescence microscopy images (Biorevo, BZ-9000, Keyence) of Jurkat cells treated with Ir complexes **4**, **5** (75 μM), **2**, **6a**, **7a**, **8**, and **9** (50 μM) for 1 h at 37 °C. (a) Bright field image of **2**, (b) emission image of **2**, (c) overlay image of (a) and (b), (d) bright field image of **4**, (e) emission image of **4**, (f) overlay image of (d) and (e), (g) bright field image of **5**, (h) emission image of **5**, (i) overlay image of (g) and (h), (j) bright field image of **6a**, (k) emission image of **6a**, (l) overlay image of (j) and (k), (m) bright field image of **7a**, (n) emission image of **7a**, (o) overlay image of (m) and (n), (p) bright field image of **8**, (q) emission image of **8**, (r) overlay image of (p) and (q), (s) bright field image of **9**, (t) emission image of **9**, (u) overlay image of (s) and (t). (v) Bright field image, (w) emission image, (x) overlay image of (v) and (w) of Jurkat cells treated with **6a** (50 μM) for 1 h at 4 °C. Excitation at 377 nm for Ir complexes, exposure time 0.25 s for (b), (q), (t), (w) and ca. 0.02 s for (e), (h), (k), (n). Scale bar (white) = 10 μm.

DOI: 10.1021/acs.bioconjchem.5b00095
Bioconjugate Chem. 2015, 26, 857−879

Chart 4

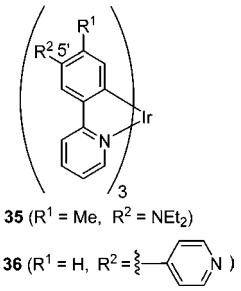

diphenyl-2*H*-tetrazolium bromide) after incubation for 16 h at 37 °C. The cell viability negligibly changed in the presence of **4** and **5**, which contain C2 and C4 alkyl linkers (entries 1 and 2 in Table 2). From Figure 3, the EC_{50} values for **6a** and **7a** were

Table 2. EC_{50} Values of Ir Complexes against Jurkat Cells[a]

entry	compound	peptide sequence (left: N-terminus)[b]	assumed net positive charge	*n*[c]	EC_{50} (μM)
1	**4**	KKGG	9	2	>50
2	**5**	KKGG	9	4	>50
3	**6a**	KKGG	9	6	16
4	**7a**	KKGG	9	8	7.3
5	**8**	KKGG	9	12	32
6	**9**	KKGG	9	16	>50
7	**6b**	D-K-D-KGG	9	6	14
8	**6c**	KKG	9	6	19
9	**6d**	GKKG	9	6	16
10	**6e**	KGKG	9	6	23
11	**6f**	KGG	6	6	>50
12	**6g**	KKKGG	12	6	10
13	**6h**	KDKKGG	9	6	>50
14	**6i**	KKDKGG	9	6	>50
15	**6j**	KKKDGG	9	6	>50
16	**7b**	KKDKGG	9	8	14
17	**10a**	KKGG	9	6	>50
18	**10b**	KKGG	9	8	>50

[a]As a racemate with respect to the stereochemistry of the Ir complex core (K: lysine, G: glycine, D: aspartic acid). [b]The stereochemistry of amino acids is the L-form unless otherwise indicated. [c]Alkyl linker length as shown in Chart 2.

determined to be 16 μM and 7.3 μM, respectively, as a racemic mixture with respect to the stereochemistry of the $Ir(tpy)_3$ unit (entries 3 and 4 in Table 2)[20] and those of **8** and **9** having C12 and C16 alkyl linker (**8**: EC_{50} = 32 μM, and **9**: EC_{50} >50 μM) are greater than those of **6a** and **7a** (entries 5 and 6 in Table 2). Since **4**, **5**, **6a**, **7a**, **8**, and **9** having KKGG peptides should have a +9 net charge at physiological pH, the linker length is important for their cytotoxicity (see the Discussion below). It should be mentioned that **8** induces negligible morphological change during the incubation for 1 h at 37 °C (Figure 2p–r) and requires longer time to induce cell death (EC_{50} is ca. 32 μM at 16 h).

For comparison, the EC_{50} values of **10a** and **10b** having a C_3-symmetric having a benzene-1,3,5-tricarboxamide center were found to be much greater than that of **6a** (entries 17 and 18 in Table 2 and Figure S5 in Supporting Information). The cytotoxic activity of the monomeric KKGG peptide **11** containing a dansylamide moiety via a C8 linker was measured by using propidium iodide (PI) that stained dead cells. Even at

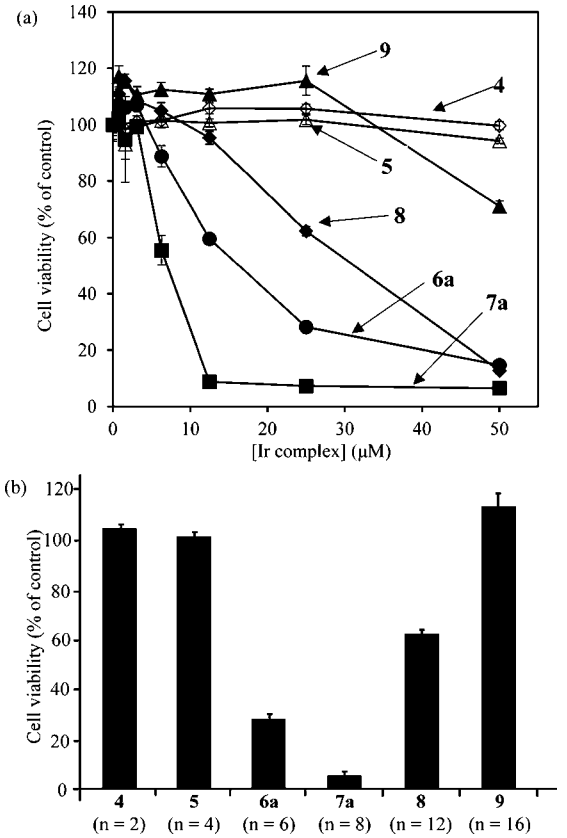

Figure 3. (a) Results of MTT assay of Jurkat cells with Ir complexes **4** (open diamonds), **5** (open triangles), **6a** (filled circles), **7a** (filled squares), **8** (filled diamonds), and **9** (filled triangles) against Jurkat cells. (b) Cell viability of Jurkat cells (% of control: 0 μM of Ir complex) in the presence of Ir complexes **4**, **5**, **6a**, **7a**, **8**, and **9** at 25 μM. Incubation times are 16 h.

150 μM, **11** induced a negligible morphological alteration and the cells were negligibly stained by PI (Figure S6 in Supporting Information).

The hydrophobicity of **4**, **5**, **6a**, **7a**, **8**, **9**, **10a**, and **10b** was roughly estimated by reverse phase HPLC (SenshuPak PEGASIL ODS, H_2O (0.1% TFA)/CH_3CN (0.1% TFA) = 90/10 to 45/55 (45 min), flow rate: 1.0 mL/min). Negligible peak (possibly due to peak broadening) was observed when neutral pH buffer (10 mM HEPES (pH 7.4)/CH_3CN) was used for HPLC. As shown in Figure S7 in Supporting Information, the retention times were 5.9 min for **10a**, 9.0 min for **4**, 12.1 min for **5**, 14.3 min for **10b**, 16.6 min for **6a**, 21.8 min for **7a**, 32.9 min for **8**, and 45.3 min for **9**, respectively, indicating that a balance between hydrophobicity and hydrophilicity of these complexes is important, although these values are retention times of Ir complexes under acidic conditions.

We next tested the cytotoxic activity of the Ir complexes **6b–g** equipped with a variety of basic peptides attached through a C6 linker (entries 7–12 in Table 2 and Figure S8 in Supporting Information). The EC_{50} of **6b** containing the D-isomer of KKGG (D-K-D-KGG) peptide was nearly the same as that of **6a** (entry 7 vs 3 in Table 2), and the values for **6c**, **6d**, and **6e**, which should possess a +9 charge at physiological pH, are almost equal to that of **6a** (entries 8–10). The Ir complex **6g** containing the KKKGG peptide (net charge: +12) had a higher activity than that of **6a**, and **6f**, which contained the KGG peptide (net charge: +6), showed a lower activity (entries 11

DOI: 10.1021/acs.bioconjchem.5b00095
Bioconjugate Chem. 2015, 26, 857–879

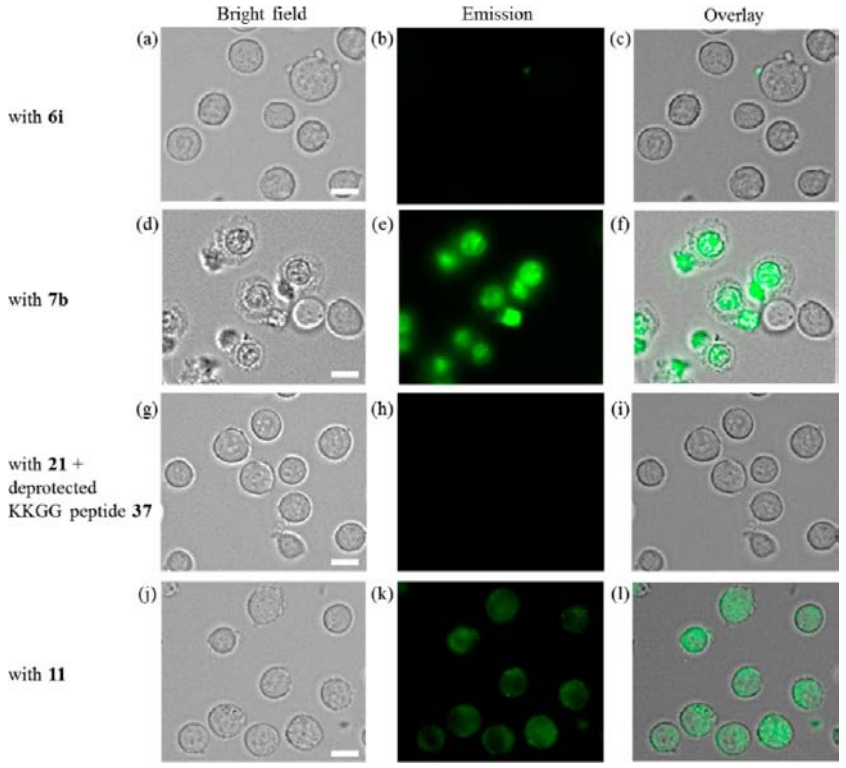

Figure 4. Luminescence microscopy images (Biorevo, BZ-9000, Keyence) of Jurkat cells treated with Ir complexes **6i** (75 μM), **7b** (50 μM), **21** (50 μM) + deprotected KKGG peptide **37** (150 μM), and **11** (225 μM) for 1 h at 37 °C. (a) Bright field image of **6i**, (b) emission image of **6i**, (c) overlay image of (a) and (b), (d) bright field image of **7b**, (e) emission image of **7b**, (f) overlay image of (d) and (e), (g) bright field image of **21** + **37**, (h) emission image of **21** + **37**, (i) overlay image of (g) and (h), (j) bright field image of **11**, (k) emission image of **11**, (l) overlay image of (j) and (k). Excitation at 377 nm for Ir complexes and an exposure time ca. 0.02 s for (b), (e), (h), and 0.25 s for (k). Scale bar (white) = 10 μm.

and 12). Therefore, to induce cell death under the above conditions, Ir complexes with a net charge of more than +9 and a C6 linker are required. However, Ir complexes **6h–j** (n = 6) having KDKKGG, KKDKGG, and KKKDGG peptides containing an aspartic acid (D) showed only negligible cytotoxic activities, although they also possess a +9 charge (entries 13–15 in Table 2 and Figure S9 in Supporting Information). On the other hand, **7b** (n = 8) containing the KKDKGG peptide exhibited a higher cytotoxic activity (EC_{50} = 14 μM) than that of **6a** (entry 16 in Table 2). The introduction of an aspartic acid unit decreased the overall hydrophobicity of **6h–j** (see Figure S7 in Supporting Information), thus reducing their cytotoxic activity, and the extension of the alkyl linker from C6 to C8 in **7b** resulted in the activity being restored. These results suggest that cell death is induced via interactions of Ir complexes with the negatively charged cell surface and/or the specific complexation with cell surface receptors, channels, or related molecules (independent of the chirality of the peptide part).

Cellular morphological changes and the luminescent staining of Jurkat cells in the presence of the Ir complexes **6i** (n = 6), **7b** (n = 8) containing the KKDKGG peptide, and dansylamide derivative **11** are shown in Figure 4. The Ir complex **6i** (75 μM) exhibited negligible morphological change and emission enhancement in the cells (Figure 4a–c). On the other hand, **7b** induced cell death and exhibited a strong green emission (Figure 4d–f). Moreover, the morphological changes observed in the presence of the Ir complex containing only a C6 linker **21** (50 μM) and the deprotected KKGG peptide **37** (150 μM) were negligible, indicating that the conjugation of the Ir complex and the cationic peptide is necessary (Figure 4g–i). For comparison, the dansylamide derivative **11** (225 μM) containing monomeric KKGG was introduced into cells, but negligible morphological change was observed, as shown in Figure 4j–l.

Selectivity of the Cytotoxic Activity against a Variety of Cancer Cells and Normal Cells. The selectivity of the cytotoxic activity of **6a** against HeLa-S3 (human epithelial carcinoma) cells, A549 (human alveolar adenocarcinoma) cells, and Molt-4 (human T-lymphocyte leukemia) cells was examined by means of MTT assay. As summarized in Figure 5a and Table 3, the EC_{50} values for **6a** against Jurkat, Molt-4, HeLa-S3, and A549 cells were in the range of 13–42 μM.[21,22] Figure S10 in Supporting Information provides information regarding cell death and the emission enhancement of Molt-4, HeLa-S3, and A549 cells after treatment with **6a** at 37 °C for 1 h.

The EC_{50} value of **6a** for normal mouse lymphocytes in 10% FCS RPMI 1640 is >50 μM (Figure 5b), which is greater than those against Jurkat and HeLa-S3 cells.[23] These phenomena may be explained by the difference in the negatively charged surface, and/or the expression levels of cell surface receptors and channels, and/or changes in membrane fluidity, and/or an increase in microvilli on the cancer cell membrane.[3e,i,l] For example, it has been reported that the surface density of negatively charged phosphatidylserine is different between cancer and normal cells.[3b,f,4]

Interaction of Ir Complexes with Cell Membrane Studied by Using Liposome and by ζ Potential Measurement of Cancer Cells. In order to study the interactions between amphiphilic Ir complexes and phospholipids in the cell membrane, we prepared giant liposomes

DOI: 10.1021/acs.bioconjchem.5b00095
Bioconjugate Chem. 2015, 26, 857–879

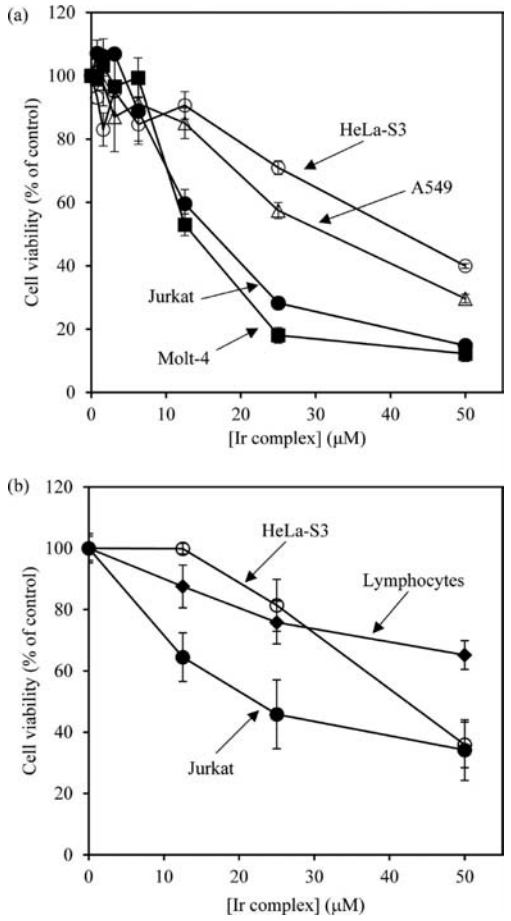

Figure 5. (a) Results of MTT assays for Ir complexes **6a** against Jurkat cells (filled circles), Molt-4 cells (filled squares), HeLa-S3 cells (open circles), and A549 cells (open triangles) in 10% FCS RPMI 1640 medium (incubation at 37 °C for 16 h). (b) Cell viability of **6a** against normal mouse lymphocytes (filled diamonds), Jurkat cells (filled circles), and HeLa-S3 cells (open circles) in 10% FCS RPMI 1640 medium (determined by PI staining after incubation at 37 °C for 1 h).

Table 3. EC_{50} Values for the Ir Complex 6a against Some Cancer Cells Determined by MTT Assay after Incubation at 37 °C for 16 h

entry	cells	EC_{50} (μM)
1	Jurkat cells	16
2	Molt-4 cells	13
3	HeLa-S3 cells	42
4	A549 cells	32

consisting of lecithin (zwitterionic phospholipids such as a phosphatidylcholine) from egg yolk as a model of a cell membrane. Phase contrast microscopic images of the giant liposomes in the presence of **5** (C4 linker) and **6a** (C6 linker) at a concentration of 75 μM (a relatively high concentration) revealed negligible morphological changes (Figure 6b and c vs 6a). On the other hand, morphology changes were observed within a few minutes after a treatment with **7a**, **8**, and **9** (Figure 6d–f). These results indicate that interactions of **5** and **6a** with phospholipids are weaker than that of **7a**, **8**, and **9**, implying that **6a** exhibits its cytotoxicity against Jurkat cells via interaction with cell membrane receptors and/or anionic molecules that are expressed on the surface of the cancer cells, rather than the direct interaction with cell membrane.

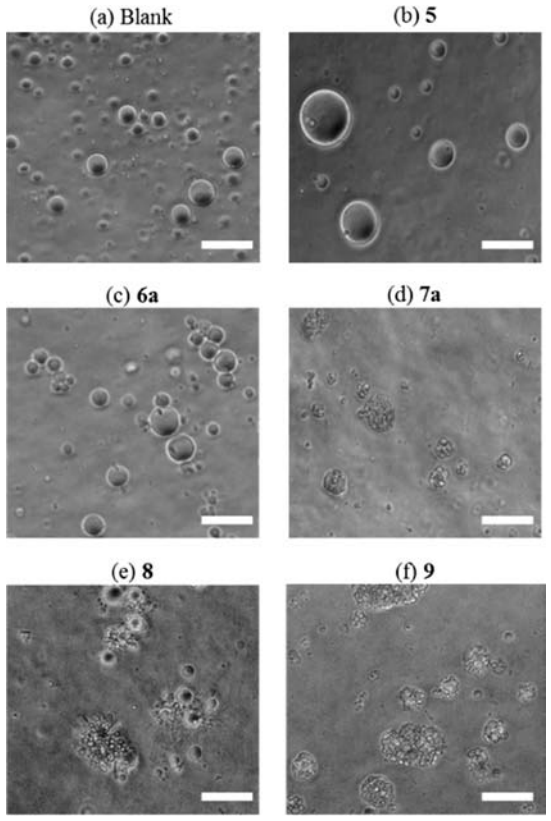

Figure 6. Giant liposomes were incubated in 10 mM HEPES at pH 7.4 with Ir complexes (75 μM). After 15 min, phase contrast images were observed on Biorevo, BZ-9000 (Keyence). (a) Blank (only buffer), (b) **5**, (c) **6a**, (d) **7a**, (e) **8**, and (f) **9**. Scale bar (white) = 50 μm.

Castanho and co-workers recently demonstrated the interaction of CAPs with cancer cells by analysis of ζ potential, which is the electrostatic potential near the surface of cells and is altered by interactions with charged compounds.[3k,24] For example, it was reported that the addition of a cationic peptide induced an increase in the negative ζ potential values of cancer cells due to the binding to the cell surface. These data prompted us to measure the effect of Ir complexes (25 μM) having a +9 net charge in PBS (10 mM, pH 7.4) at 37 °C on the ζ potential of Jurkat cells. As shown in Figure S11 in Supporting Information, the addition of **6a** (25 μM) reduced the magnitude of the negative charge of the Jurkat cells from −11.2 ± 1.4 mV to −5.35 ± 0.37 mV, from which the $\Delta(\zeta$ potential) is calculated to be ca. +5.9 mV, possibly due to its electrostatic interaction with the cell surface. In addition, **5** (−8.98 ± 0.74 mV, $\Delta(\zeta$ potential) = +2.2 mV) and **6i** (−6.51 ± 0.65 mV, $\Delta(\zeta$ potential) = +4.7 mV) also reduced the magnitude of the ζ potential of Jurkat cells to almost same extent as **6a**. The ζ potentials of HeLa-S3 cells ($\Delta(\zeta$ potential) = +4.3 mV) and A549 cells ($\Delta(\zeta$ potential) = +5.3 mV) were also reduced to about −6 mV. The ζ potential of normal mouse lymphocytes is −17.8 ± 8.4 mV,[24a,b] and the increase in the ζ potential of normal mouse lymphocytes in the presence of **6a** was much greater than those of other cancer cells. These results suggest that the decrease in the ζ potentials of each cell by Ir complexes is not correlated with their cytotoxicity, a finding that is consistent with previous reports.[3k,24]

Mechanistic Studies of Cell Death Induced by 6a. Typical time-lapse images (0–30 min) of Jurkat cells treated with **6a** (75 μM) show a morphological change accompanied

DOI: 10.1021/acs.bioconjchem.5b00095
Bioconjugate Chem. 2015, 26, 857–879

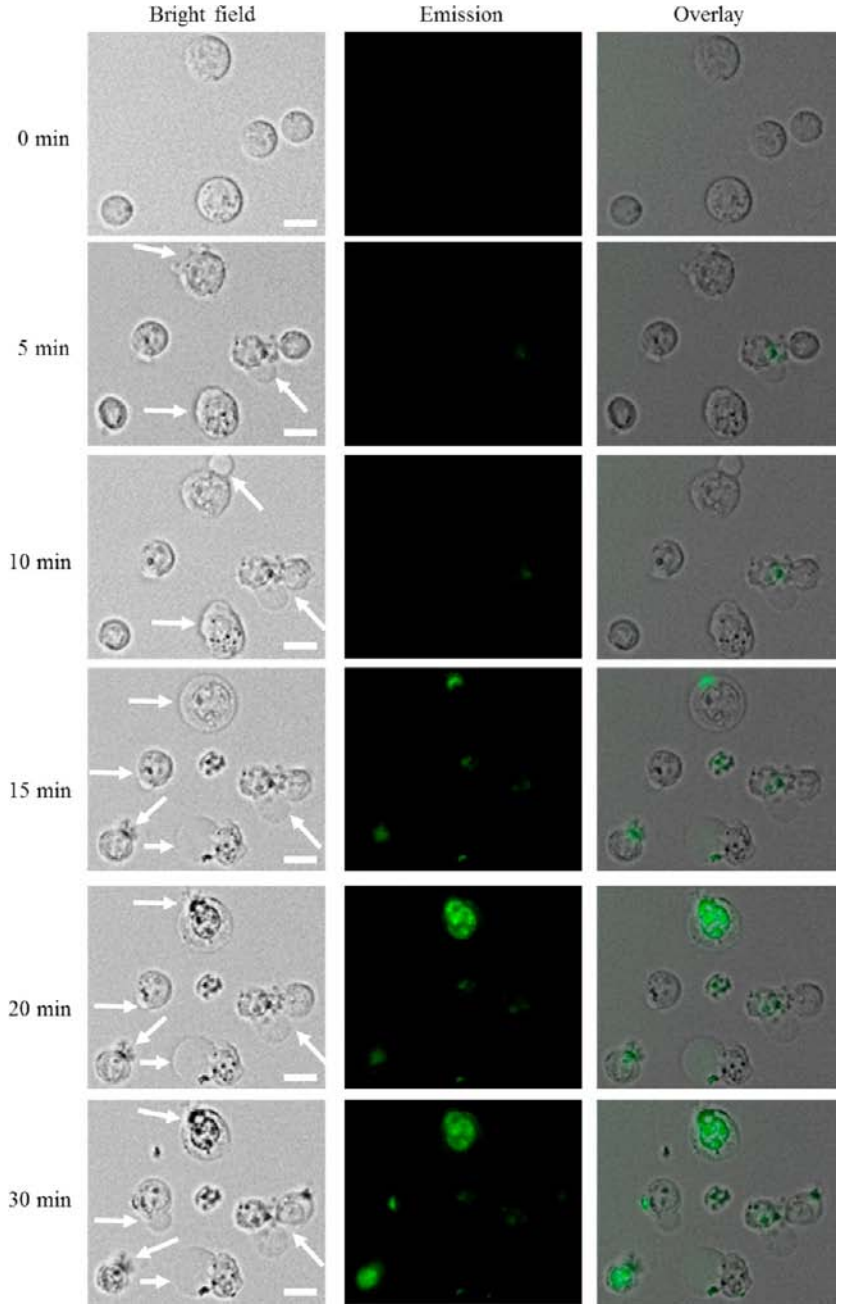

Figure 7. Typical time-lapse images (Biorevo, BZ-9000, Keyence) of Jurkat cells treated with **6a** (75 μM) at 37 °C. Morphological change with swelling and blebbing are shown in white arrows. Scale bar (white) = 10 μm. Excitation at 377 nm for **6a** (exposure time 0.01 s).

by bubble-like swelling and blebbing, followed by membrane disruption (Figure 7 and movie S1 in Supporting Information). After that, the green emission of Ir complex **6a** is observed around the damaged membrane (15−20 min in Figure 7) and then accumulates in the nucleus after 20−30 min.[25]

The co-staining study of Jurkat cells with **6a** (75 μM) and PI (30 μM) was performed. PI shows a strong red emission by intercalating with DNA in the nucleus by passing through the damaged membrane of dead cells. The photos in Figure S12 in Supporting Information show a typical bright field image of Jurkat cells (Figure S12a), a **6a**-stained emission image of Jurkat cells (Figure S12b), a PI emission image of Jurkat cells (Figure S12c), an overlay image of Figure S12a and S12b (Figure S12d), an overlay image of Figure S12a and S12c (Figure S12e), and an overlay image of Figure S12b and S12c (Figure S12f), in which the area of the emission for **6a** mostly overlapped with that of PI, indicating that **6a** had accumulated in the nuclei of dead cells. Moreover, a substantial overlap between the emission of **6a** and PI was also observed in a costaining study of normal mouse lymphocytes (Figure S13 in Supporting Information). These data suggest that +9 charged **6a** might have accumulated in dead cells and/or interacted with negatively charged biological species such as DNA in the nucleus through electrostatic interactions, possibly at the later stages of cell death. Indeed, a ca. 2.5-fold increase in the emission intensity of **6a** (0.5 μM) at pH 7.4 (10 mM HEPES (I = 0.1 ($NaNO_3$)) was observed upon the addition of calf thymus DNA (ctDNA) (5.0 μM in phosphate) (Figure S14 in Supporting Information) and a similar behavior was observed for **7a**.

DOI: 10.1021/acs.bioconjchem.5b00095
Bioconjugate Chem. 2015, 26, 857−879

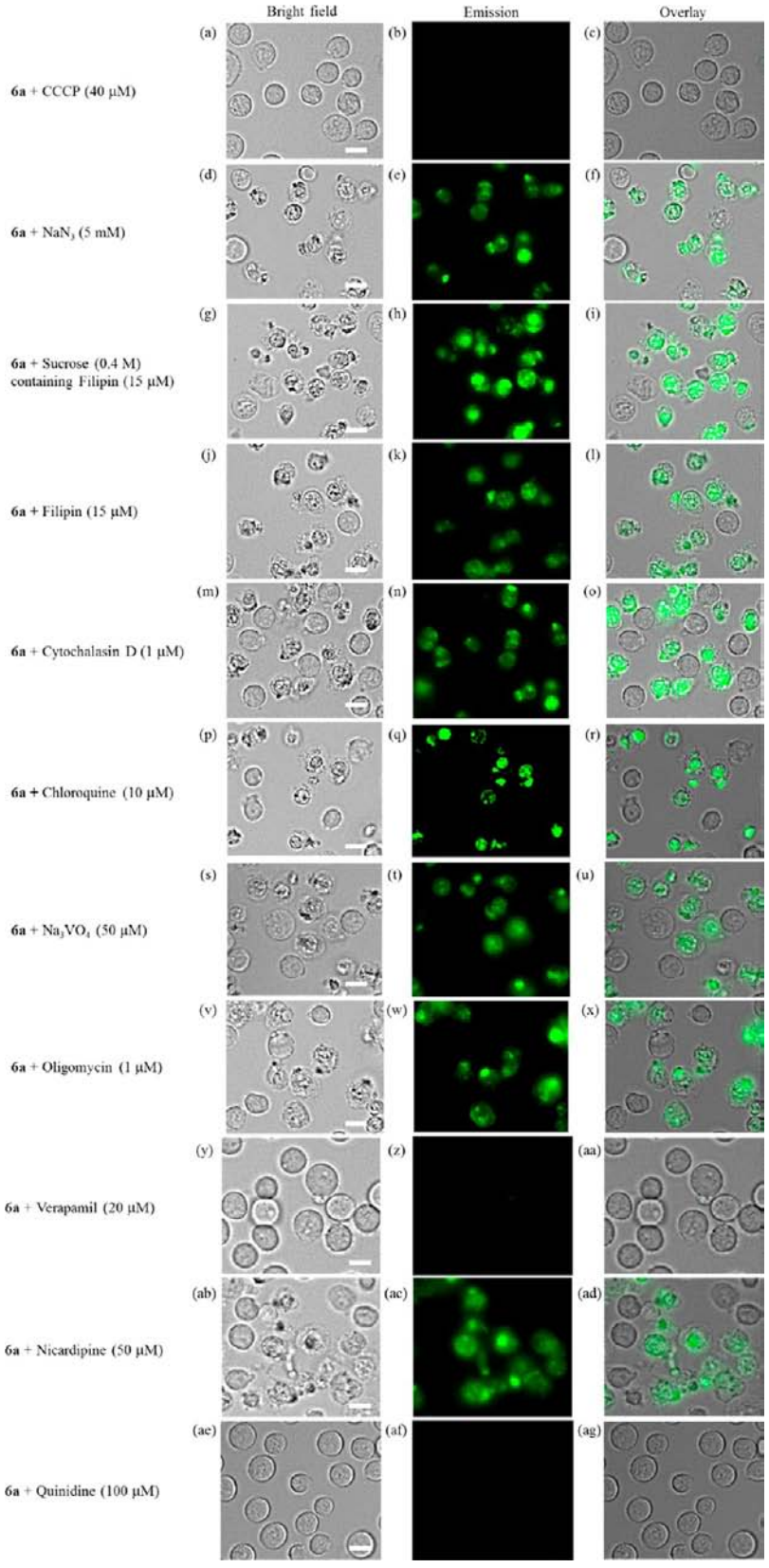

Figure 8. Typical luminescence microscopy images (Biorevo, BZ-9000, Keyence) of Jurkat cells treated with Ir complexes **6a** (50 μM) in the presence of CCCP (a–c), NaN_3 (d–f), sucrose + filipin (g–i), filipin (j–l), cytochalasin D (m–o), chloroquine (p–r), Na_3VO_4 (s–u), oligomycin (v–x),verapamil (y–aa), nicardipine (ab–ad), and quinidine (ae–ag) at 37 °C for 1 h. Excitation at 377 nm for **6a** (exposure time ca. 0.02 s). Scale bar = 10 μm.

DOI: 10.1021/acs.bioconjchem.5b00095
Bioconjugate Chem. 2015, 26, 857–879

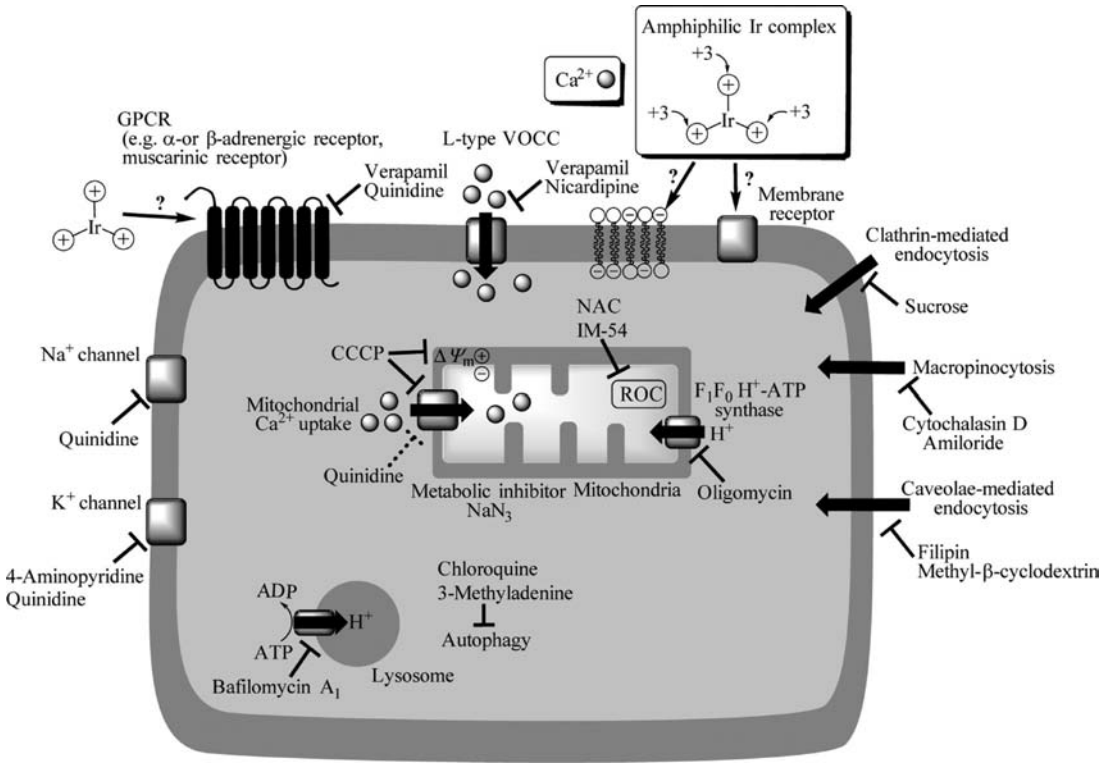

Figure 9. Possible reactive sites of the inhibitors used in this study. VOCC: voltage-operated Ca^{2+} channel.

The aforementioned results indicate that cell death induced by Ir complexes proceeds not only via their interaction with the cell membrane but also by triggering intracellular events. To investigate whether cell death induced by Ir complexes is apoptosis or necrosis, we carried out MTT assay of **6a** (75 μM) in the presence of Z-VAD-fmk,[26] which is a broad caspase inhibitor (its structure is shown in Figure S15 in Supporting Information). TNF-related apoptosis-inducing ligand (TRAIL)[27] was used as a positive control. Although Z-VAD-fmk inhibited the apoptosis induced by TRAIL, cell death induced by **6a** was not inhibited (Figure S16 in Supporting Information). In addition, the cytotoxic activity of **6a** was not inhibited by necrostatin-1, a necroptosis inhibitor,[28] IM-54, which inhibits necrosis induced by oxidative stress,[29] and a ROS scavenger (*N*-acetyl-L-cysteine (NAC)), respectively (Figures S16 in Supporting Information). In addition, the cytotoxic activities of **6a** against wild type and Bcl-2 overexpressing Molt-4 cells[30] were nearly equal (Figure S17 in Supporting Information). These results suggest that cell death induced by cationic amphiphilic Ir complexes can be classified as necrotic cell death rather than apoptosis.

As described above, the cytotoxicity of **6a** is inhibited at 4 °C (Figure 2v–x), suggesting that **6a**-induced cell death is mediated via an energy-dependent pathway. In order to investigate this possibility, the cell death of Jurkat cells with **6a** was examined in the presence of a variety of inhibitors such as carbonyl cyanide 3-chlorophenylhydrazone (CCCP) (a mitochondrial uncoupling reagent),[31] NaN_3 (a metabolic inhibitor), sucrose (an inhibitor of clathrin-mediated endocytosis), filipin and methyl-β-cyclodextrin (MβCD) (inhibitors of caveolae-mediated endocytosis),[32] sucrose + filipin, cytochalasin D, amiloride (inhibitors of macropinocytosis),[33] 3-methyladenine[34] and chloroquine[35] (inhibitors of autophagy), bafilomycin A1 (an inhibitor of vacular ATPase (V-ATPase)),[36] oligomycin (an inhibitor of the mitochondrial F_1/F_0-ATP synthase to cause ATP depletion),[37] sodium orthovanadate (Na_3VO_4) (an inhibitor of ATPase),[38] and 4-aminopyridine (K^+ channel blocker) (Figure 8 and Figure S18 in Supporting Information). The structures of these inhibitors are shown in Figure S15 in Supporting Information and the most likely reactive sites of these drugs are summarized in Figure 9. Moreover, Hoechst 33342 (a minor groove-binder of DNA with adenine-thymine selectivity), and spermidine (a substrate of the polyamine transporter, used as a competitive substrate)[39] were also tested. It was confirmed that these agents themselves did not induce cell death at the concentrations used in the experiments.

Interestingly, the morphological change (and cell death) of the Jurkat cells by **6a** was substantially inhibited only by CCCP (40 μM) as shown in Figure 8a–c[40] (the cytotoxicity of **6a** against Molt-4 cells is also inhibited at 4 °C and by CCCP, Figure S19 in Supporting Information). The cell death induced by **6a** was inhibited by verapamil (20 μM) (L-type voltage-operated Ca^{2+} channel blocker) as shown in Figure 8y–aa,[41] and not by nicardipine (50 μM), which is also an L-type voltage-operated Ca^{2+} channel blocker (Figure 8ab–ad).[41] The use of a Ca^{2+}-free RPMI1640 based buffer (Figure S18) failed to stop the cell death, suggesting that the entry of extracellular Ca^{2+} is not a critical factor in cell death. In addition, cell death induced by **6a** was inhibited by treatment with quinidine (100 μM), which is not only a Na^+ and K^+ channel blocker but also an antagonist of α-adrenergic receptors,[42] a muscarinic receptor,[43] and an inhibitor of the mitochondrial uptake of Ca^{2+} (Figure 8ae–ag).[44] Inhibition of **6a**-induced cell death by CCCP, verapamil, and quinidine was supported by PI staining experiments under the same conditions (Figure S20 in Supporting Information).

DOI: 10.1021/acs.bioconjchem.5b00095
Bioconjugate Chem. 2015, 26, 857–879

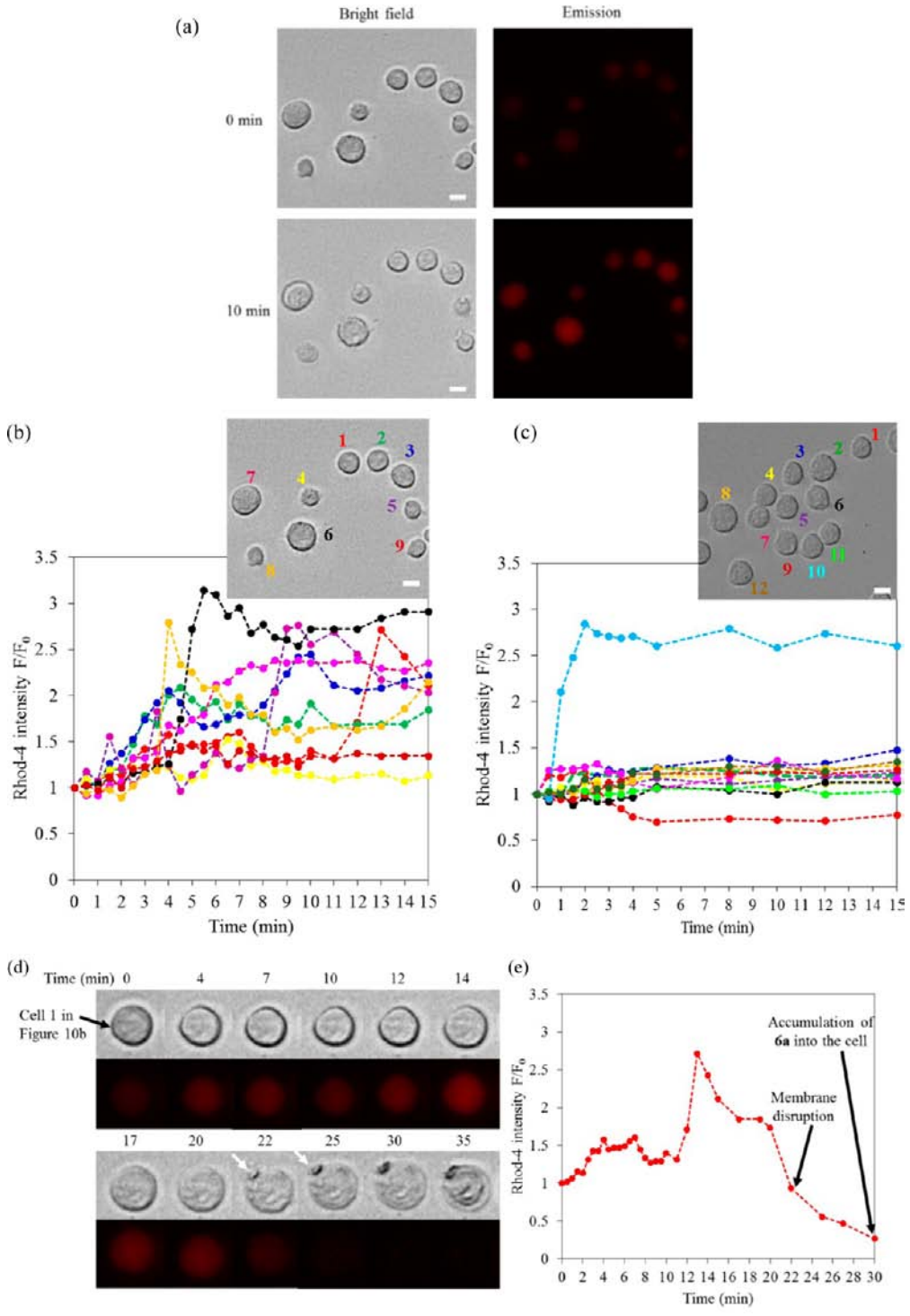

Figure 10. (a) Typical luminescence images (Biorevo, BZ-9000, Keyence) of Rhod-4 loaded Jurkat cells treated with **6a** (50 μM). Excitation at 540 nm for Rhod-4. Scale bar (white) = 10 μm. (b) and (c) Time course of fluorescent change of Rhod-4 loaded cells (F/F_0) after treatment with **6a** (50 μM) (b) and **5** (50 μM) (c). Photos show ca. 0 min after treatment with **6a** or **5**. Curves in (b) and (c) depict the change of the emission of Rhod-4 of each cell (cell 1 (red filled circles, red dashed line), 2 (green filled circles, green dashed line), 3 (blue filled circle, blue dashed line), 4 (yellow filled circles, yellow dashed line), 5 (purple filled circles, purple dashed line), 6 (black filled circles, black dashed line), 7 (pink filled circle, pink dashed line), 8 (orange filled circles, orange dashed line), 9 (brown filled circles, brown dashed line), 10 (light blue filled circles, light blue dashed line), 11 (yellow green filled circles, yellow green dashed line), and 12 (beige filled circles, beige dashed line)). Representative time-lapse images (d) and time course of fluorescent change of Rhod-4 (e) of cell 1 in (b) (red filled circles, red dashed line) after treatment with **6a** (50 μM). White arrows in Figure (d) indicate the observation of membrane disruption. F_0: initial emission intensity of Rhod-4, F: emission intensity of Rhod-4 after treatment with Ir complex.

It has been reported that CCCP compromises the membrane potential of mitochondria, resulting in a decrease in ATP production and the inhibition of mitochondrial calcium (Ca^{2+}) uptake.[31,45,46] Therefore, we measured the membrane potential

DOI: 10.1021/acs.bioconjchem.5b00095
Bioconjugate Chem. 2015, 26, 857−879

of mitochondria in the presence of **6a** by staining with TMRM (tetramethyl rhodamine methyl ester).[47] However, flow cytometry measurements revealed that **6a** had a negligible effect against the mitochondrial membrane potential of Jurkat cells (Figure S21 in Supporting Information).

An observation of Figure 2 and Figure 8 indicates that some cells had survived after the treatment with **6a** (Figures 2l and 8f,i,l,o,r,u,x,ad). Thus, we suspected the existence of a relationship between the cytotoxicity of **6a** and the cell cycle. The cell cycle of Jurkat cells was arrested in the G_1/S phase by treatment with thymidine and in the G_2/M phase by a nocodazole treatment (Figure S22 in Supporting Information).[48] As shown in Figure S23 in Supporting Information, a similar morphological change and emission enhancement were observed in both cases after treatment with **6a**. Therefore, we assume that the cytotoxicity of **6a** against Jurkat cells is independent of the cell cycle.

Concerning the Mechanism of Cell Death Focused on Ca^{2+}-Dependent Pathway. The aforementioned results of the induction of cell death of Jurkat and related cells induced by amphiphilic Ir complexes can be summarized as follows:

1. Ir complexes containing KKGG sequences exhibit considerable cytotoxicity against Jurkat cells, and a greater than +9 net charge and an appropriate length of alkyl chain (C6−C8) is required for activity (Figures 2 and 3 and Table 2). Covalent bonding between the peptide with Ir complexes is essential (Figure 4g−i). The data suggest a balance between hydrophobicity and hydrophilicity is important for the cytotoxicity of these complexes (Figure S7).

2. Ir complex **6a** exhibited considerable cytotoxicity against cancer cells such as Jurkat, Molt-4, HeLa-S3, and A549 cells (Figure 5a) and cytotoxicity of **6a** against normal mouse lymphocytes is lower than those against Jurkat and HeLa-S3 cells (Figure 5b).

3. Giant liposomes underwent negligible morphological changes in the presence of **6a**, suggesting that **6a** interacts weakly with the zwitterionic phospholipids in membranes (Figure 6).

4. Jurkat cells treated with **6a** at 37 °C undergo a morphological change accompanied by bubble-like swelling and blebbing, followed by membrane disruption and the accumulation of **6a** in the cell, resulting in a strong emission in the dead cells (Figure 7 and movie S1 in Supporting Information). At 4 °C, **6a** is localized mainly on/in the cell membranes of Jurkat cells (Figure 2v−x) without altering their morphology, suggesting that **6a** initially interacts with the cell membrane and then induces cell death.

5. Cell death induced by **6a** is not inhibited by Z-VAD-fmk (pan-caspase inhibitor), necrostain-1 (necroptosis inhibitor), NAC, and IM-54 (ROS scavengers), indicative of necrosis. The results of various inhibitors as shown in Figure 8 and Figure S18 suggest that **6a**-induced cell death proceeds via an energy independent pathway. In addition, **6a**-induced cell death is inhibited by CCCP (an uncoupling reagent and inhibition of mitochondrial Ca^{2+} uptake) (Figure 8a−c), verapamil (L-type voltage-operated Ca^{2+} channel blocker) (Figure 8y−aa), and quinidine (Figure 8ae−ag), and not by a variety of inhibitors, as shown in Figure 8 and Figure S18.

6. It is unlikely that the cytotoxicity of **6a** against Jurkat cells is dependent on the cell cycle (Figure S23).

This information suggests that the amphiphilic Ir complex **6a** interacts directly or indirectly with anionic molecules on the cell surface and/or membrane receptors, thus triggering the intracellular events related to Ca^{2+}.[49] Because Ca^{2+} is a well-known second messenger with a pivotal role in cell death, we anticipated that it would participate in the cell death mechanism induced by **6a**. Paredes-Gamero and co-workers recently reported that gomesin (a cationic antimicrobial peptide isolated from hemocytes from the Brazilian spider) induces an increase in intracellular Ca^{2+} levels that participates in the necrotic cell death of CHO cells.[50a] In this report, it is described that gomesin enters the cells and induces the release of Ca^{2+} from the endoplasmic reticulum (ER), the disruption of ER, mitochondrial Ca^{2+} overload and oxidative stress, resulting in necrosis of CHO cells. In addition, gomesin induces an increase of cytosolic Ca^{2+} levels, causing apoptosis and necroptosis in K562 cells (a human erythroleukemia cell line), not via oxidative stress.[50b]

The findings reported here indicate the cationic amphiphilic Ir complex **6a** initially binds to the cell surface and stimulates intracellular events regarding necrotic cell death. Since CCCP inhibits mitochondrial Ca^{2+} uptake by depolarizing the mitochondrial membrane potential (Figure 9),[45] **6a** may induce a mitochondrial Ca^{2+} overload, which is counterbalanced by CCCP.[45,51]

Verapamil has a variety of effects as an inhibitor not only as a L-type voltage-operated Ca^{2+} channel blocker (Figure 9), but also as an inhibitor of the G-protein coupled receptor (GPCR) such as α- and β-adrenergic receptors,[52] muscarinic receptor,[53] and serotonin receptor.[54] From the results for verapamil (Figure 8y−aa) and quinidine (Figure 8ae−ag), we assume that **6a**-induced cell death mediated by adrenergic receptors is unlikely, because (−)-epinephrine (5 mM) itself exhibits negligible cytotoxicity and has a negligible effect on **6a**-induced cell death (Figure S18). Although it is not easy to quantify the effect of quinidine, which is reported to affect some receptors and channels on the cell membrane and intracellular molecules, the possibility that quinidine is involved in the inhibition of mitochondrial Ca^{2+} uptake induced by **6a** (Figure 9) cannot be excluded.[44]

An increase of cytosolic Ca^{2+} concentration was assessed by fluorescent microscopy. Jurkat cells were stained with Rhod-4/AM, which is mainly localized in the cytoplasm. As shown in Figure 10a and b, the fluorescent intensity of Rhod-4 was enhanced after treatment with **6a** (50 μM), indicating that **6a** induces an increase in cytosolic Ca^{2+} levels. As shown in representative time-lapse images (cell 1 in Figure 10b) of Figure 10d and e, most (ca. 75%) of the **6a**-treated Jurkat cells showed a Ca^{2+} response (Figure 10a and b) and then underwent morphological changes, followed by the disappearance of Rhod-4 emission. In contrast, the effect of **5** (50 μM), which has only a negligible effect on cell death (see Figure 2g−i and Figure 3), was weak (Figure 10c). A careful observation of morphological and luminescent images of **6a**-treated cells suggest that the membranes of the cells collapse after the Ca^{2+} response (Figure 10e). Therefore, we conclude that cell death induced by the amphiphilic Ir complexes studied in this work is strongly correlated with the induction of an intracellular Ca^{2+} response, although the details of this process remain to be studied.

CONCLUSIONS

We report herein on the design and synthesis of cationic amphiphilic tris-cyclometalated iridium(III) complexes as inducers and detectors of cell death. The findings indicate that Ir complexes that contain highly cationic peptides

DOI: 10.1021/acs.bioconjchem.5b00095
Bioconjugate Chem. 2015, 26, 857−879

including KKGG sequences exhibit considerable cytotoxicity against Jurkat cells. The structure−cytotoxicity relationship of Ir complexes reveals that both more than a +9 net charge and alkyl chains with an appropriate length (C6−C8) are necessary for achieving this activity. While weak interactions of Ir complexes **4** and **5** having shorter alkyl linkers (C2 or C4) with negatively charged cell surface showed negligible cytotoxicity, **6a** and **7a**, which contain C6 and C8 linkers, exhibit a high degree of cytotoxicity. On the other hand, **8** and **9**, with C12 and C16 linkers, become localized on the cell surface and, as a result, show a lower (or slower) cytotoxicity. A lower activity was also observed in Ir complex **6h−j** containing aspartic acid in the peptide sequence and the benzene-1,3,5-tricarboxamide derivatives **10a** and **10b**. Moreover, it was found that **6a** exhibits a high cytotoxicity against cancer cells such as Jurkat cells, Molt-4 cells, HeLa-S3 cells, A549 cells, and a lower cytotoxicity against normal lymphocytes than those against Jurkat and HeLa-S3 cells. Mechanistic studies suggest that Ir complexes such as **6a−e**, **6g**, and **7a−b** interact with anionic molecules on the cell surface and/or membrane receptors to trigger the Ca^{2+} dependent pathway and an intracellular Ca^{2+} response, resulting in necrosis accompanied by membrane disruption. The isolation and identification of target molecules of Ir complexes by photoaffinity labeling[55] and the development of a detailed understanding of the intracellular events activated by Ir complexes and the accumulation of Ir complexes in dead cells is a future project.

These results may provide useful information for understanding the mechanism responsible for the cell death of amphiphiles, the future design and synthesis of luminescent cationic amphiphilic anticancer agents in bioorganometallics,[11,56] biomedicinal science, and related fields.

EXPERIMENTAL PROCEDURES

General Information. All reagents and solvents were of the highest commercial quality and were used without further purification, unless otherwise noted. Anhydrous *N*,*N*-dimethylformamide (DMF) was obtained by distillation from calcium hydride. All aqueous solutions were prepared using deionized and distilled water. UV−vis spectra were recorded on a JASCO V-550 spectrophotometer at 25 °C. Emission spectra were recorded on a JASCO FP-6200 spectrofluorometer at 25 °C. IR spectra were recorded on a PerkinElmer FT-IR spectrophotometer (Spectrum100) at room temperature. Melting points were measured using a Yanaco MP-J3Micro Melting Point apparatus and are uncorrected. ^{1}H (300 and 400 MHz) and ^{13}C (75 and 100 MHz) NMR spectra were recorded on a JEOL Always 300 spectrometer and a JEOL Lamda 400 spectrometer, respectively. Luminescence imaging studies were performed using fluorescent microscopy (Biorevo, BZ-9000, Keyence). Tetramethylsilane (TMS) was used as an internal reference for ^{1}H and ^{13}C NMR measurements in $CDCl_3$ and CD_3OD. 3-(Trimethylsilyl)-propionic-2,2,3,3-d_4 acid (TSP) sodium salt was used as an external reference for ^{1}H NMR measurement in D_2O. Mass spectral measurements were performed on a JEOL JMS-SX102A and Varian TQ-FT. Mass of some tris-cyclometalated Ir complexes are observed as $[M]^+$ (rather than $[M + H]^+$) in ESI mode (Varian TQ-FT).[14] Fast atom bombardment (FAB) mass spectrum was recorded on JEOL JMS-SX102A. Elemental analyses were performed on a PerkinElmer CHN 2400 series II CHNS/O analyzer. Lyophilization was performed with freeze-dryer FD-5N (EYELA). Thin-layer chromatographies (TLC) and silica gel column chromatographies were performed using Merck Art 5554 (silica gel) TLC plate and Fuji Silysia Chemical FL-100D, respectively. MTT (3-(4,5-dimethyl-2-thiazolyl)-2,5-diphenyl-2*H*-tetrazolium bromide), hoechst 33342 were purchased from Dojindo. Z-VAD-fmk (Z-Val-Ala-Asp(OMe)-fluoromethylketone) was purchased from Peptide Institute. Necrostatin-1 and IM-54 were purchased from Enzo Life Sciences. Propidium iodide and NaN_3 were purchased from Nacalai tesque. TRAIL/Apo2L (human, recombinant), *N*-acetyl-L-cysteine, 3-methyladenine, chloroquine diphosphate, verapamil hydrochloride, nicardipine hydrochloride, and lecithin from egg yolk were purchased from WAKO Pure Chemical Industries. Quinidine and 4-aminopyridine were purchased from TCI. The oligomycin complex was purchased from Cayman Chemical Co. CCCP (carbonyl cyanide 3-chlorophenylhydrazone), bafilomycin A1, amiloride hydrochloride, and DNA sodium salt from calf thymus were purchased from Sigma-Aldrich. TMRM (tetramethyl rhodamine methyl ester) was purchased from Cosmo Bio Co. Quest Rhod-4/AM was purchased from AAT Bioquest. HPLC experiments were carried out using a system consisting of two PU-980 intelligent HPLC pumps (JASCO, Japan), a UV-970 intelligent UV−visible detector (JASCO), a Rheodine injector (Model No. 7125), and a Chromatopak C-R6A (Shimadzu, Japan). For analytical HPLC, a SenshuPak Pegasil ODS column (Senshu Scientific Co., Ltd.) (4.6ϕ × 250 mm, No. 07051001) was used. For preparative HPLC, a SenshuPak Pegasil ODS SP100 column (Senshu Scientific Co., Ltd.) (20ϕ × 250 mm, No. 1302014G) was used. GPC experiments were carried out using a system consisting of a POMP P-50 (Japan Analytical Industry Co., Ltd.), a UV/vis DETECTOR S-3740 (Soma, Japan), a Manual Sample Injector 7725i (Rheodyne, USA), a MDL-101 1 PEN RECORDER (Japan Analytical Industry Co., Ltd.), equipped with two preparative GPC, JAIGEL-1H and JAIGEL-2 (Japan Analytical Industry Co., Ltd.) (20ϕ × 600 mm, No. A605201 and A605204) were used.

Ir Complex ***15***. *N*,*N*-Diisopropylethylamine (DIEA) (0.19 g, 1.5 mmol), PyBOP (0.38 g, 0.73 mmol), and mono-Boc-protected hexamethylenediamine[57] (0.31 g, 1.5 mmol) were added to a solution of **12** (99 mg, 0.12 mmol) in freshly distilled DMF (3 mL). The reaction mixture was stirred at room temperature for 36 h, and then concentrated under reduced pressure. The remaining residue was purified by silica gel column chromatography ($CHCl_3$/MeOH, 1/0 to 50/1 to 0/1) and gel permeation chromatography ($CHCl_3$) and recrystallized from Hexanes/$CHCl_3$ to afford the Boc protected **15** (92 mg, 55%) as a yellow solid. Mp 153 °C (decompose). IR (ATR): ν = 3315, 2929, 2849, 1689, 1630, 1587, 1521, 1472, 1391, 1365, 1251, 1165, 1070, 889, 780, 749 cm^{-1}. ^{1}H NMR (300 MHz, $CDCl_3$/TMS): δ = 7.87 (t, J = 8.1 Hz, 3H), 7.70 (s, 3H), 7.61 (dd, J = 8.1 Hz, 1.8 Hz, 3H), 7.38 (d, J = 4.8 Hz, 3H), 6.86 (t, J = 5.7 Hz, 3H), 6.69 (s, 3H), 5.88−5.76 (m, 3H), 4.62−4.46 (m, 3H), 3.47−3.35 (m, 6H), 3.18−3.05 (m, 6H), 2.24 (s, 9H), 1.51−1.26 (m, 51H) ppm. ^{13}C NMR (100 MHz, CD_3OD/TMS): δ = 174.5, 166.9, 165.4, 158.5, 148.3, 143.2, 140.2, 138.0, 137.5, 130.2, 123.7, 123.3, 120.1, 79.8, 41.2, 40.7, 30.9, 30.4, 28.8, 27.8, 27.5, 20.0 ppm. ESI-MS (m/z) Calcd for $C_{72}H_{96}{}^{191}IrN_9O_9Ir$ $[M]^+$: 1421.6931. Found: 1421.6891. Anal. Calcd for $C_{72}H_{96}IrN_9O_9$: C, 60.74; H, 6.80; N, 8.85%. Found: C, 60.54; H, 7.00; N, 8.72%.

Ir complexes **13**, **14**, **16**, **17**, and **18** were prepared in a manner similar to that described for **15**.

Ir Complex ***13***. A yellow solid (51% from **12**). Mp 182 °C (decompose). IR (ATR): ν = 3298, 2977, 1704, 1624, 1585,

DOI: 10.1021/acs.bioconjchem.5b00095
Bioconjugate Chem. 2015, 26, 857−879

1506, 1475, 1428, 1392, 1366, 1253, 1163, 1072, 993, 892, 860, 779, 751, 726 cm^{-1}. ^1H NMR (300 MHz, CD_3OD/TMS): δ = 8.21 (t, J = 4.2 Hz, 3H), 8.05 (d, J = 6.3 Hz, 3H), 7.81 (s, 3H), 7.68 (dd, J = 6.2 Hz, 0.9 Hz, 3H), 7.46 (d, J = 3.6 Hz, 3H), 6.93 (t, J = 4.5 Hz 3H), 6.70 (s, 3H), 3.46−3.36 (m, 6H), 3.29−3.20 (m, 6H), 2.13 (s, 9H), 1.40 (s, 27H) ppm. ^{13}C NMR (100 MHz, CD_3OD/TMS): δ = 174.7, 166.9, 165.9, 158.7, 148.3, 143.3, 140.3, 138.0, 137.8, 129.7, 124.0, 123.4, 120.2, 80.1, 41.1, 40.9, 28.8, 20.2 ppm. ESI-MS (m/z) Calcd for $C_{60}H_{72}{}^{191}IrN_9O_9$ $[M]^+$: 1256.5177. Found: 1256.5155. Anal. Calcd for $C_{60}H_{72}IrN_9O_9{\cdot}0.5CHCl_3$: C, 55.25; H, 5.56; N, 9.59%. Found: C, 54.88; H, 5.64; N, 9.41%.

Ir Complex ***14***. A yellow solid (49% from **12**). Mp 172 °C (decompose). IR (ATR): ν = 3302, 2933, 1692, 1637, 1601, 1517, 1473, 1428, 1393, 1366, 1254, 1167, 1070, 893, 781, 752 cm^{-1}. ^1H NMR (300 MHz, $CDCl_3$/TMS): δ = 7.87 (d, J = 8.2 Hz, 3H), 7.70 (s, 3H), 7.60 (t, J = 7.1 Hz, 3H), 7.38 (d, J = 5.1 Hz, 3H), 6.86 (t, J = 6.4 Hz, 3H), 6.70 (s, 3H), 5.93 (s, 3H), 4.65 (s, 3H), 3.50−3.34 (m, 6H), 3.15 (d, J = 5.8 Hz, 6H), 2.23 (s, 9H), 1.66 (s, 15H), 1.43 (s, 27H) ppm. ^{13}C NMR (100 MHz, CD_3OD/TMS): δ = 174.7, 167.0, 165.7, 158.7, 148.4, 143.4, 140.3, 138.1, 137.6, 130.2, 123.8, 123.4, 120.2, 79.9, 41.0, 40.4, 28.8, 28.5, 27.7, 20.0 ppm. ESI-MS (m/z) Calcd for $C_{66}H_{84}N_9O_9{}^{191}Ir$ $[M]^+$: 1337.60275. Found: 1337.59924. Anal. Calcd for $C_{66}H_{84}IrN_9O_9{\cdot}2H_2O$: C, 57.62; H, 6.45; N, 9.16%. Found: C, 57.64; H, 6.30; N, 9.10%.

Ir Complex ***16***. A yellow solid (46% from **12**). Mp 135 °C (decompose). IR (ATR): ν = 3297, 2928, 1691, 1634, 1602, 1532, 1472, 1429, 1392, 1365, 1253, 1168, 1070, 781, 749 cm^{-1}. ^1H NMR (400 MHz, CD_3OD/TMS): δ = 7.99 (d, J = 8.3 Hz, 3H), 7.76−7.63 (m, 6H), 7.46 (d, J = 5.5 Hz, 3H), 6.94 (t, J = 6.4 Hz, 3H), 6.74 (s, 3H), 3.34−3.26 (m, 6H), 3.00 (t, J = 7.0 Hz, 6H), 2.13 (s, 9H), 1.66−1.52 (m, 6H), 1.51−1.25 (m, 57H) ppm. ^{13}C NMR (100 MHz, CD_3OD/TMS): δ = 174.6, 167.0, 165.6, 158.7, 148.5, 143.4, 140.3, 138.1, 137.6, 130.3, 123.8, 123.5, 120.1, 79.8, 73.0, 41.3, 40.8, 30.9, 30.4, 30.3, 28.8, 28.0, 27.8, 20.0 ppm. ESI-MS (m/z) Calcd for $C_{78}H_{108}N_9O_9{}^{191}IrNa$ $[M + Na]^+$: 1528.7771. Found: 1528.7768. Anal. Calcd for $C_{78}H_{108}IrN_9O_9$: C, 62.13; H, 7.22; N, 8.36%. Found: C, 62.39; H, 6.97; N, 8.37%.

Ir Complex ***17***. A yellow solid (64% from **12**). Mp 173 °C (decompose). IR (ATR): ν = 3300, 2925, 2854, 1690, 1631, 1601, 1529, 1472, 1427, 1391, 1365, 1252, 1169, 1070, 891, 781, 748 cm^{-1}. ^1H NMR (400 MHz, CD_3OD/TMS): δ = 8.00 (d, J = 8.2 Hz, 3H), 7.80−7.62 (m, 6H), 7.47 (d, J = 5.3 Hz, 3H), 6.94 (t, J = 6.4 Hz, 3H), 6.74 (s, 3H), 3.39−3.24 (m, 6H), 2.99 (t, J = 7.0 Hz, 6H), 2.13 (s, 9H), 1.69−1.51 (m, 6H), 1.51−1.20 (m, 81H) ppm. ^{13}C NMR (100 MHz, CD_3OD/TMS): δ = 174.6, 167.1, 165.6, 158.7, 148.5, 143.4, 140.3, 138.1, 137.6, 130.3, 123.8, 123.5, 120.1, 79.8, 41.4, 40.8, 31.0, 30.7, 30.7, 30.4, 30.4, 28.8, 28.1, 27.8, 20.0 ppm. ESI-MS (m/z) Calcd for $C_{90}H_{132}N_9O_9{}^{191}IrNa$ $[M + Na]^+$: 1696.9654. Found: 1696.9646. Anal. Calcd for $C_{90}H_{132}IrN_9O_9$: C, 64.49; H, 7.94; N, 7.52%. Found: C, 64.84; H, 8.01; N, 7.72%.

Ir Complex ***18***. A yellow solid (53% from **12**). Mp 130 °C (decompose). IR (ATR): ν = 3281, 2922, 2852, 1723, 1627, 1601, 1536, 1469, 1430, 1368, 1288, 1261, 1126, 1072, 1037, 892, 843, 782, 747, 722 cm^{-1}. ^1H NMR (300 MHz, $CDCl_3$/TMS): δ = 7.87 (d, J = 8.5 Hz, 3H), 7.71 (s, 3H), 7.61 (t, J = 7.0 Hz, 3H), 7.39 (d, J = 5.5 Hz, 3H), 6.86 (t, J = 6.0 Hz, 3H), 6.69 (s, 3H), 5.76 (s, 3H), 4.66−4.38 (m, 3H), 3.51−3.32 (m, 6H), 3.19−2.99 (m, 6H), 2.24 (s, 9H), 1.44 (s, 42H), 1.25 (s, 69H) ppm. ^{13}C NMR (100 MHz, CD_3OD/TMS): δ = 174.7, 167.1, 165.6, 158.7, 148.5, 143.4, 140.3, 138.1, 137.6, 130.3, 123.8, 123.4, 120.1, 79.8, 41.4, 40.8, 31.0, 30.8, 30.7, 30.4, 28.8, 28.1, 27.9, 20.0 ppm. ESI-MS (m/z) Calcd for $C_{102}H_{157}N_9O_9{}^{191}Ir$ $[M + H]^+$: 1843.1733. Found: 1843.1705. Anal. Calcd for $C_{102}H_{156}IrN_9O_9$: C, 66.42; H, 8.52; N, 6.83%. Found: C, 66.15; H, 8.61; N, 6.88%.

Ir Complex ***6a***. A mixture of TMSCl (65 mg, 1.4 mmol) and NaI (0.21 g, 1.4 mmol) in CH_3CN (3 mL) was added to a suspension of Boc protected **15** (65 mg, 45 μmol) in CH_3CN (10 mL). The mixture was stirred at room temperature for 10 min and sonicated for 2 min. The insoluble compound was centrifuged and washed with CH_3CN to give **21** as the HI salt. The product was purified by preparative HPLC (H_2O (0.1% TFA)/CH_3CN (0.1% TFA) = 80/20 to 50/50 (30 min), t_r = 21 min, 6.0 mL/min), lyophilized to give **21** as a yellow solid (41 mg, 62% as 3TFA salt). Mp 274 °C (decompose). IR (ATR): ν = 2934, 1675, 1601, 1532, 1473, 1426, 1302, 1264, 1200, 1179, 1129, 1070, 892, 836, 799, 783, 751, 722 cm^{-1}. ^1H NMR (300 MHz, CD_3OD/TMS): δ = 8.02 (d, J = 6.0 Hz, 3H), 7.80−7.65 (m, 6H), 7.47 (d, J = 4.2 Hz, 3H), 6.96 (t, J = 4.8 Hz, 3H), 6.73 (s, 3H), 3.40−3.25 (m, 6H), 2.91 (t, J = 5.4 Hz, 6H), 2.13 (s, 9H), 1.75−1.55 (m, 12H), 1.55−1.35 (m, 12H) ppm. ^{13}C NMR (100 MHz, CD_3OD/TMS): δ = 174.6, 166.8, 165.5, 148.4, 143.3, 140.2, 138.0, 137.5, 130.1, 123.6, 123.4, 120.0, 40.6, 40.5, 30.2, 28.5, 27.4, 27.0, 20.0 ppm. ESI-MS (m/z) Calcd for $C_{57}H_{73}N_9O_3{}^{191}Ir$ $[M + H]^+$: 1122.5437. Found: 1122.5435. Anal. Calcd for $C_{57}H_{72}IrN_9O_3{\cdot}3CF_3CO_2H{\cdot}5.5H_2O$: C, 48.36; H, 5.54; N, 8.06%. Found: C, 48.06; H, 5.16; N, 7.86%.

DIEA (8.8 mg, 68 μmol), PyBop (35 mg, 68 μmol), and protected KKGG peptide **25** (9.4 mg, 14 μmol) were added to a solution of **21** (5.0 mg, 3.4 μmol) in dist. DMF (1 mL). The reaction mixture was stirred at room temperature for 16 h. It was then concentrated under reduced pressure and purified by silica gel column chromatography ($CHCl_3$/MeOH = 20/1 to 10/1) to afford the protected compound (13 mg) as a yellow powder. A mixture of TMSCl (0.15 g, 1.4 mmol) and NaI (0.20 g, 1.4 mmol) in CH_3CN (4.5 mL) was added to a mixture of the protected compound in CH_3CN (1.5 mL). The reaction mixture was stirred at room temperature for 2 h. After deprotection, the insoluble compound was isolated by centrifugation and washed with CH_3CN. The resulting residue was purified by preparative HPLC (H_2O (0.1% TFA)/CH_3CN (0.1% TFA) = 80/20 to 60/40 (30 min), t_r = 23 min, 6.0 mL/min), lyophilized to give **6a** as a yellow solid (5.0 mg, 29% as 9TFA salt from **15**). ^1H NMR (400 MHz, D_2O/TSP): δ = 8.06 (d, J = 8.0 Hz, 3H), 7.83 (t, J = 8.0 Hz, 3H), 7.79 (s, 3H), 7.70 (d, J = 5.6 Hz, 3H), 7.10 (t, J = 6.6 Hz, 3H), 6.59 (s, 3H), 4.37 (t, J = 6.6 Hz, 3H), 4.01−3.98 (m, 3H), 3.98 (s, 6H), 3.88 (s, 6H), 3.39−3.36 (m, 6H), 3.26−3.19 (m, 6H), 2.99 (q, J = 7.6 Hz, 12H), 2.12 (s, 9H), 1.95−1.60 (m, 30H), 1.60−1.30 (m, 30H) ppm. ESI-MS (m/z) Calcd for $C_{105}H_{164}N_{27}O_{15}{}^{191}Ir$ $[M + 2H]^{2+}$: 1117.1248. Found: 1117.1248.

Ir complexes **4**, **5**, **6b**−**j**, **7a**−**b**, **8**, and **9** were prepared in a manner similar to that described for **6a**.

Ir Complex ***19***. A yellow solid (61% as 3TFA salt from **13**). Mp 270 °C (decompose). IR (ATR): ν = 2930, 1676, 1600, 1535, 1474, 1426, 1303, 1265, 1200, 1129, 1072, 917, 838, 786, 752, 723 cm^{-1}. ^1H NMR (300 MHz, CD_3OD/TMS): δ = 8.08 (d, J = 6.0 Hz, 3H), 7.90 (s, 3H), 7.74 (dd, J = 6.0 Hz, 0.9 Hz, 3H), 7.50 (d, J = 3.9 Hz, 3H), 6.99 (t, J = 4.8 Hz, 3H), 6.71 (s, 3H), 3.68−3.54 (m, 6H), 3.17 (t, J = 4.5 Hz, 6H), 2.16 (s, 9H) ppm. ^{13}C NMR (100 MHz, CD_3OD/TMS): δ = 175.3, 166.7,

DOI: 10.1021/acs.bioconjchem.5b00095
Bioconjugate Chem. 2015, 26, 857−879

166.6, 148.4, 143.6, 140.5, 138.3, 138.1, 128.5, 124.1, 123.6, 120.2, 40.9, 38.7, 20.3 ppm. ESI-MS (m/z) Calcd for $C_{45}H_{48}{}^{191}IrN_9O_3Na$ $[M + Na]^+$: 976.3378. Found: 976.3374. Anal. Calcd for $C_{45}H_{48}IrN_9O_3{\cdot}3CF_3CO_2H{\cdot}4.5H_2O$: C, 44.44; H, 4.39; N, 9.15%. Found C, 44.04; H, 4.02; N, 8.90%.

Ir Complex ***4***. A yellow powder (28% as 9TFA salt from **13**). ^{1}H NMR (400 MHz, D_2O/TSP): δ = 8.09 (d, J = 8.8 Hz, 3H), 7.84 (t, J = 8.8 Hz, 3 H), 7.83 (s, 3H), 7.69 (d, J = 5.6 Hz, 3H), 7.11 (t, J = 6.6 Hz), 6.61 (s, 3H), 4.37−4.32 (m, 3H), 4.04 (t, J = 6.6 Hz, 3H), 3.95−3.90 (m, 12H), 3.55−3.49 (m, 12H), 3.55−3.49 (m, 12H), 2.13 (s, 9H), 1.93−1.90 (m, 6H), 1.85−1.60 (m, 18H), 1.50−1.35 (m, 12H) ppm. ESI-MS (m/z) Calcd for: $C_{93}H_{140}N_{27}O_{15}{}^{191}Ir$ $[M+2H]^{2+}$: 1033.0309. Found: 1033.0304.

Ir Complex ***20***. A yellow solid (59% as 3TFA salt from **14**). Mp 179 °C (decompose). IR (ATR): ν = 2931, 1674, 1601, 1533, 1473, 1426, 1303, 1265, 1199, 1176, 1129, 1070, 893, 837, 799, 783, 751, 722 cm^{-1}. ^{1}H NMR (300 MHz, CD_3OD/TMS): δ = 8.09 (d, J = 8.1 Hz, 3H), 8.02−7.70 (m, 6H), 7.49 (d, J = 5.4 Hz, 3H), 6.99 (t, J = 6.3 Hz, 3H), 6.72 (s, 3H), 3.40 (d, J = 6.5 Hz, 6H), 3.00 (t, J = 6.6 Hz, 6H), 2.14 (s, 9H), 1.74 (s, 12H) ppm. ^{13}C NMR (100 MHz, CD_3OD/TMS): δ = 174.7, 166.8, 165.8, 148.4, 143.4, 140.3, 138.1, 1376, 129.8, 123.7, 123.5, 120.1, 40.4, 39.9, 27.5, 26.0, 20.1 ppm. FAB-MS (m/z) Calcd for $C_{51}H_{60}N_9O_3{}^{191}Ir$ $[M]^+$: 1037.4425. Found: 1037.4425.

Ir Complex ***5***. A yellow solid (14% as 9TFA salt from **14**). ^{1}H NMR (400 MHz, D_2O/TSP): δ = 8.07 (d, J = 8.0 Hz, 3H), 7.83 (t, J = 8.0 Hz, 3 H), 7.79 (s, 3H), 7.69 (d, J = 5.2 Hz, 3H), 7.10 (t, J = 6.4 Hz), 6.59 (s, 3H), 4.36 (t, J = 7.2 Hz, 3H), 4.05 (t, J = 6.6 Hz, 3H), 3.96 (s, 6H), 3.91 (s, 6H), 3.41−3.36 (m, 6H), 3.32−3.22 (m, 6H), 3.02−2.95 (m, 12H), 2.73 (s, 9H), 1.95−1.80 (m, 6H), 1.80−1.60 (m, 30H), 1.50−1.35 (m, 12H) ppm. ESI-MS (m/z) Calcd for $C_{99}H_{152}$ $N_{27}O_{15}{}^{191}Ir$ $[M+2H]^{2+}$: 1075.0770. Found: 1075.0778.

Ir Complex ***6b***. A yellow amorphous (33% as 9TFA salt from **15**). ^{1}H NMR (400 MHz, D_2O/TSP): δ = 8.07 (d, J = 8.8 Hz, 3H), 7.83 (t, J = 7.8 Hz, 3H), 7.79 (s, 3H), 7.70 (d, J = 5.6 Hz, 3H), 7.10 (t, J = 6.6 Hz, 3H), 6.59 (s, 3H), 4.37 (t, J = 6.2 Hz, 3H), 4.05 (t, J = 6.4 Hz, 3H), 3.98 (s, 6H), 3.88 (s, 6H), 3.37 (t, J = 7.0 Hz, 6H), 3.28−3.19 (m, 6H), 3.03−2.97 (m, 12H), 2.12 (s, 9H), 1.95−1.75 (m, 12H), 1.75−1.35 (m, 48H) ppm. ESI-MS (m/z) Calcd for: $C_{105}H_{165}N_{27}O_{15}{}^{191}Ir$ $[M+3H]^{3+}$: 745.0856. Found: 745.0858.

Ir Complex ***6c***. A yellow solid (35% as 9TFA salt from **15**). ^{1}H NMR (400 MHz, D_2O/TSP): δ = 8.06 (d, J = 8.0 Hz, 3H), 7.83 (t, J = 8.0 Hz, 3H), 7.79 (s, 3H), 7.69 (d, J = 5.6 Hz, 3H), 7.10 (t, J = 6.6 Hz, 3H), 6.59 (s, 3H), 4.35 (t, J = 7.2 Hz, 3H), 4.03 (t, J = 6.4 Hz, 3H), 3.90−3.84 (m, 6H), 3.38−3.36 (m, 6H), 3.26−3.20 (m, 6H), 3.02−2.97 (m, 12H), 2.12 (s, 9H), 1.95−1.78 (m, 12H), 1.75−1.63 (m, 18H), 1.59−1.36 (m, 30H) ppm. ESI-MS (m/z) Calcd for: $C_{99}H_{155}N_{24}O_{12}{}^{191}Ir$ $[M+2H]^{2+}$: 1031.5926. Found: 1031.5928.

Ir Complex ***6d***. A yellow amorphous (13% as 9TFA salt from **15**). ^{1}H NMR (400 MHz, D_2O/TSP): δ = 8.07 (d, J = 8.0 Hz, 3H), 7.84 (t, J = 8.0 Hz, 3H), 7.79 (s, 3H), 7.70 (d, J = 5.2 Hz, 3H), 7.10 (t, J = 6.6 Hz, 3H), 6.60 (s, 3H), 4.35 (t, J = 6.8 Hz, 3H), 4.30 (t, J = 7.4 Hz, 3H), 3.87 (s, 6H), 3.87−3.78 (m, 6H), 3.40−3.34 (m, 6H), 3.87 (s, 6H), 3.87−3.78 (m, 6H), 3.40−3.34 (m, 6H), 3.23 (t, J = 6.6 Hz, 6H), 2.98 (t, J = 7.6 Hz, 12H), 2.13 (s, 9H), 1.85−1.60 (m, 30H), 1.60−1.35 (m, 30H) ppm. ESI-MS (m/z) Calcd for: $C_{105}H_{164}N_{27}O_{15}{}^{191}Ir$ $[M+2H]^{2+}$: 1117.1248. Found: 1117.1264.

Ir Complex ***6e***. A yellow solid (25% as 9TFA salt from **15**). ^{1}H NMR (400 MHz, D_2O/TSP): δ = 8.07 (d, J = 8.4 Hz, 3H), 7.83 (t, J = 7.0 Hz, 3H), 7.79 (s, 3H), 7.70 (d, J = 5.2 Hz, 3H), 7.10 (t, J = 6.2 Hz, 3H), 6.59 (s, 3H), 4.34−4.28 (m, 3H), 4.10−4.05 (m, 9H), 3.84−3.82 (m, 6H), 3.39−3.36 (m, 6H), 3.22 (t, J = 6.8 Hz, 6H), 3.04−2.96 (m, 12H), 2.12 (s, 9H), 2.00−1.90 (m, 6H), 1.80−1.60 (m, 24H), 1.60−1.32 (m, 30H) ppm. ESI-MS (m/z) Calcd for: $C_{105}H_{164}N_{27}O_{15}{}^{191}Ir$ $[M+2H]^{2+}$: 1117.1248. Found: 1117.1264.

Ir Complex ***6f***. A yellow solid (56% as 6TFA salt from **15**). ^{1}H NMR (400 MHz, D_2O/TSP): δ = 8.07 (d, J = 8.8 Hz, 3H), 7.83 (t, J = 8.0 Hz, 3H), 7.79 (s, 3H), 7.70 (d, J = 4.4 Hz, 3H), 7.10 (t, J = 6.2 Hz, 3H), 6.59 (s, 3H), 4.08 (t, J = 6.8 Hz, 6H), 4.04 (m, 6H), 3.88 (brs, 6H), 3.37 (t, J = 6.8 Hz, 6H), 3.23 (t, J = 7.0 Hz, 6H), 3.01 (t, J = 7.6 Hz, 6H), 2.12 (s, 9H), 1.96−1.93 (m, 6H), 1.75−1.60 (m, 12H), 1.60−1.30 (m, 24H) ppm. ESI-MS (m/z) Calcd for: $C_{87}H_{129}N_{21}O_{12}{}^{191}Ir$ $[M+3H]^{3+}$: 616.9906. Found: 616.9902.

Ir Complex ***6g***. A yellow amorphous (24% as 12TFA salt from **15**). ^{1}H NMR (400 MHz, D_2O/TSP): δ = 8.06 (d, J = 8.8 Hz, 3H), 7.83 (t, J = 8.0 Hz, 3H), 7.79 (s, 3H), 7.69 (d, J = 5.2 Hz, 3H), 7.10 (t, J = 6.6 Hz, 3H), 6.59 (s, 3H), 4.36 (t, J = 7.2 Hz, 3H), 4.31 (brt, J = 5.0 Hz, 3H), 4.03 (t, J = 6.6 Hz, 3H), 3.98 (s, 6H), 3.89 (s, 6H), 3.37 (t, J = 6.8 Hz, 6H), 3.25−3.19 (m, 6H), 3.04−2.98 (m, 18H), 2.12 (s, 9H), 1.95−1.60 (m, 42H), 1.60−1.30 (m, 36H) ppm. ESI-MS (m/z) Calcd for: $C_{123}H_{202}N_{33}O_{16}{}^{191}Ir$ $[M+4H]^{4+}$: 655.1372. Found: 655.1370.

Ir Complex ***6h***. A yellow solid (35% as 12TFA salt from **15**). ^{1}H NMR (300 MHz, D_2O/TSP): δ = 8.05 (d, J = 8.1 Hz, 3H), 7.82 (t, J = 7.5 Hz, 3H), 7.78 (s, 3H), 7.69 (d, J = 5.4 Hz, 3H), 7.09 (t, J = 6.2 Hz, 3H), 6.59 (s, 3H), 4.34−4.25 (m, 6H), 4.04 (t, J = 6.4 Hz, 3H), 3.94 (m, 6H), 3.86 (s, 6H), 3.39−3.35 (m, 6H), 3.25−3.15 (m, 6H), 3.05−2.80 (m, 27H), 2.12 (s, 9H), 2.00−1.60 (m, 42H), 1.60−1.30 (m, 36H) ppm. ESI-MS (m/z) Calcd for $C_{135}H_{215}N_{36}O_{27}{}^{191}Ir$ $[M+2H]^{2+}$: 1481.8083. Found: 1481.8076.

Ir Complex ***6i***. A yellow solid (33% as 12TFA salt from **15**). ^{1}H NMR (400 MHz, D_2O/TSP): δ = 8.05 (d, J = 8.0 Hz, 3H), 7.82 (t, J = 8.0 Hz, 3H), 7.78 (s, 3H), 7.69 (d, J = 5.2 Hz, 3H), 7.09 (t, J = 6.6 Hz, 3H), 6.59 (brs, 3H), 4.37 (t, J = 7.0 Hz, 3H), 4.30−4.26 (m, 3H), 4.04 (t, J = 6.4 Hz, 3H), 3.93 (m, 6H), 3.85 (s, 6H), 3.40−3.30 (m, 6H), 3.22 (t, J = 6.8 Hz, 6H), 3.04−2.75 (m, 27H), 2.12 (s, 9H), 1.95−1.60 (m, 42H), 1.55−1.30 (m, 36H) ppm. ESI-MS (m/z) Calcd for $C_{135}H_{216}N_{36}O_{27}{}^{191}Ir$ $[M+3H]^{3+}$: 988.2072. Found: 988.2075.

Ir Complex ***6j***. A yellow solid (16% as 12TFA salt from **15**). ^{1}H NMR (300 MHz, D_2O/TSP): δ = 8.06 (d, J = 8.2 Hz, 3H), 7.82 (t, J = 8.2 Hz, 3H), 7.79 (s, 3H), 7.69 (d, J = 5.4 Hz, 3H), 7.09 (t, J = 6.5 Hz, 3H), 6.59 (s, 3H), 4.37−4.27 (m, 6H), 4.04 (t, J = 6.6 Hz, 3H), 3.94 (s, 6H), 3.86 (s, 6H), 3.40−3.35 (m, 6H), 3.22 (t, J = 6.6 Hz, 6H), 3.04−2.95 (m, 21H), 2.87−2.82 (m, 6H), 2.12 (s, 9H), 1.95−1.60 (m, 42H), 1.60−1.30 (m, 36H) ppm. ESI-MS (m/z) Calcd for $C_{135}H_{216}N_{36}O_{27}{}^{191}Ir$ $[M+3H]^{3+}$: 988.2043. Found: 988.2075.

Ir Complex ***22***. A yellow solid (54% as 3TFA salt from **16**). Mp 146 °C (decompose). IR (ATR): ν = 3284, 3027, 2930, 2859, 1674, 1602, 1532, 1473, 1426, 1302, 1263, 1199, 1178, 1127, 1070, 893, 837, 799, 783, 751, 722 cm^{-1}. ^{1}H NMR (300 MHz, CD_3OD/TMS): δ = 8.06 (d, J = 8.3 Hz, 3H), 7.75 (t, J = 6.9 Hz, 6H), 7.48 (d, J = 5.5 Hz, 3H), 6.99 (t, J = 6.4 Hz, 3H),

DOI: 10.1021/acs.bioconjchem.5b00095
Bioconjugate Chem. 2015, 26, 857−879

6.74 (s, 3H), 3.36 (d, J = 7.1 Hz, 6H), 2.91 (t, J = 7.6 Hz, 6H), 2.13 (s, 9H), 1.64 (s, 12H), 1.51−1.32 (m, 24H) ppm. ^{13}C NMR (100 MHz, CD_3OD/TMS): δ = 174.5, 166.8, 165.4, 148.3, 143.2, 140.1, 137.9, 137.3, 130.1, 123.5, 123.3, 119.9, 40.5, 40.5, 30.2, 29.8, 29.8, 28.3, 27.7, 27.1, 19.8 ppm. ESI-MS (m/z) Calcd for $C_{63}H_{85}N_9O_3{}^{191}Ir$ $[M + H]^+$: 1206.6354. Found: 1206.6376.

Ir Complex ***7a***. A yellow solid (7% as 9TFA salt from **16**). ^{1}H NMR (400 MHz, D_2O/TSP): δ = 8.06 (d, J = 8.0 Hz, 3H), 7.83 (t, J = 8.0 Hz, 3H), 7.79 (s, 3H), 7.70 (d, J = 4.8 Hz, 3H), 7.10 (t, J = 6.8 Hz, 3H), 6.58 (s, 3H), 4.38 (t, J = 7.2 Hz, 3H), 4.05 (t, J = 6.4 Hz, 3H), 3.98 (s, 6H), 3.86 (s, 6H), 3.40−3.35 (m, 6H), 3.20−3.15 (m, 6H), 3.03−2.98 (m, 12H), 2.12 (s, 9H), 2.00−1.60 (m, 30H), 1.50−1.33 (m, 42H) ppm. ESI-MS (m/z) Calcd for $C_{111}H_{178}N_{27}O_{15}{}^{191}Ir$ $[M+4H]^{4+}$: 580.0897. Found: 580.0895.

Ir Complex ***7b***. A yellow powder (14% as 12TFA salt from **16**). ^{1}H NMR (400 MHz, D_2O/TSP): δ = 8.06 (d, J = 8.0 Hz, 3H), 7.83 (t, J = 8.0 Hz, 3H), 7.79 (s, 3H), 7.70 (d, J = 5.2 Hz, 3H), 7.09 (t, J = 5.8 Hz, 3H), 6.58 (s, 3H), 4.38 (t, J = 7.2 Hz, 6H), 4.30−4.29 (m, 3H), 4.05 (t, J = 6.2 Hz, 3H), 3.94 (s, 6H), 3.84 (s, 6H), 3.38−3.35 (m, 6H), 3.20−3.12 (m, 6H), 3.04−2.77 (m, 27H), 2.12 (s, 9H), 1.95−1.63 (m, 36H), 1.47−1.33 (m, 54H) ppm. ESI-MS (m/z) Calcd for $C_{141}H_{228}N_{36}O_{27}{}^{191}Ir$ $[M+3H]^{3+}$: 1016.2370. Found: 1016.2388.

Ir Complex ***23***. A yellow solid (71% as 3TFA salt from **17**). Mp 112 °C (decompose). IR (ATR): ν = 3041, 2927, 2856, 1675, 1602, 1532, 1472, 1428, 1303, 1266, 1201, 1180, 1132, 1071, 896, 838, 799, 783, 752, 723 cm^{-1}. ^{1}H NMR (400 MHz, CD_3OD/TMS): δ = 8.01 (d, J = 8.3 Hz, 3H), 7.80−7.64 (m, 6H), 7.46 (d, J = 5.0 Hz, 3H), 6.95 (t, J = 6.2 Hz, 3H), 6.72 (s, 3H), 3.39−3.21 (m, 6H), 2.86 (t, J = 7.6 Hz, 6H), 2.12 (s, 9H), 1.70−1.50 (m, 8H), 1.45−1.23 (m, 48H) ppm. ^{13}C NMR (100 MHz, CD_3OD/TMS): δ = 174.7, 167.0, 165.6, 148.5, 143.4, 140.3, 138.1, 137.5, 130.3, 123.7, 123.5, 120.1, 40.8, 40.7, 30.6, 30.6, 30.5, 30.4, 30.3, 30.2, 28.5, 28.0, 27.4, 20.0 ppm. ESI-MS (m/z) Calcd for $C_{75}H_{109}N_9O_3{}^{191}Ir$ $[M + H]^+$: 1374.8244. Found: 1374.8254.

Ir Complex ***8***. A yellow solid (42% as 9TFA salt from **17**). ^{1}H NMR (300 MHz, CD_3OD/TMS): δ = 8.03 (d, J = 8.4 Hz, 3H), 7.76−7.71 (m, 3H), 7.73 (s, 3H), 7.47 (d, J = 5.1 Hz, 3H), 6.97 (t, J = 6.4 Hz, 3H), 6.72 (s, 3H), 4.36 (t, J = 6.9 Hz, 3H), 4.02−3.85 (m, 15H), 3.17 (t, J = 6.9 Hz, 6H), 2.96 (q, J = 6.8 Hz, 12H), 2.13 (s, 9H), 1.92−1.49 (m, 42H), 1.36−1.30 (m, 54H) ppm. ESI-MS (m/z) Calcd for $C_{123}H_{202}N_{27}O_{15}{}^{191}Ir$ $[M+4H]^{4+}$: 622.1362. Found: 622.1364.

Ir Complex ***24***. A yellow solid (58% as 3TFA salt from **18**). Mp 155 °C (decompose). IR (ATR): ν = 3305, 2920, 2852, 1675, 1603, 1527, 1471, 1427, 1299, 1253, 1202, 1184, 1134, 1070, 897, 841, 800, 778, 753, 723 cm^{-1}. ^{1}H NMR (300 MHz, CD_3OD/TMS): δ = 8.02 (d, J = 8.2 Hz, 3H), 7.86−7.61 (m, 6H), 7.47 (d, J = 5.5 Hz, 3H), 6.96 (t, J = 6.0 Hz, 3H), 6.73 (s, 3H), 2.89 (t, J = 7.5 Hz, 6H), 2.65 (s, 6H), 2.13 (s, 9H), 1.72−1.49 (m, 12H), 1.47−1.16 (m, 72H) ppm. ESI-MS (m/z) Calcd for $C_{87}H_{133}N_9O_3{}^{191}Ir$ $[M + H]^+$: 1543.0157. Found: 1543.0132.

Ir Complex ***9***. A yellow solid (20% as 9TFA salt from **18**). ^{1}H NMR (300 MHz, CD_3OD/TMS): δ = 8.03 (d, J = 9.0 Hz, 3H), 7.75−7.72 (m, 3H), 7.72 (s, 3H), 7.47 (d, J = 5.1 Hz, 3H), 6.96 (t, J = 6.5 Hz, 3H), 6.72 (s, 3H), 4.35 (t, J = 7.2 Hz, 3H), 3.99−3.90 (m, 9H), 3.85 (s, 6H), 3.17 (t, J = 6.9 Hz, 6H), 2.98−2.90 (m, 12H), 2.12 (s, 9H), 1.90−1.86 (m, 12H), 1.78−1.47 (m, 30H), 1.36−1.30 (m, 78H) ppm. ESI-MS (m/z) Calcd for $C_{135}H_{225}N_{27}O_{15}{}^{191}Ir$ $[M+3H]^{3+}$: 885.2418. Found: 885.2421.

Measurements of UV/vis Absorption and Luminescence Spectra. UV/vis spectra were recorded on a JASCO V-550 UV/vis spectrophotometer and emission spectra were recorded on a JASCO FP-6200 spectrofluorometer at 25 °C. Concentrations of all the Ir complexes in stock solutions (PBS: phosphate buffer saline) were determined based on a molar extinction coefficient of 380 nm ($\varepsilon_{380\ nm}$ = (1.08 ± 0.07) × 10^4 M^{-1} cm^{-1}) of **19** and **21** that were characterized by elemental analysis. Sample aqueous solutions in quartz cuvettes equipped with Teflon septum screw caps were degassed by Ar bubbling through the solution for 10 min prior to making the luminescence measurements. The quantum yields for luminescence (Φ) were determined by comparison with the integrated corrected emission spectrum of a quinine sulfate standard, whose emission quantum yield in 0.1 M H_2SO_4 was assumed to be 0.55[58] (excitation at 366 nm). Equation 1 was used in calculating the emission quantum yields, in which Φ_s and Φ_r denote the quantum yields of the sample and reference compound, η_s and η_r are the refractive indexes of the solvents used for the measurements of the sample and reference, and A_s and A_r are the absorbance of the sample and the reference, and I_s and I_r stand for the integrated areas under the emission spectra of the sample and reference, respectively (all of the Ir compounds were excited at 366 nm for luminescence measurements in this study).

$$\Phi_s = \Phi_r(\eta_s^2 A_r I_s)/(\eta_r^2 A_s I_r) \quad (1)$$

The luminescence lifetimes of sample solutions in degassed aqueous solutions at 298 K were measured on a TSP1000-M-PL (Unisoku, Osaka, Japan) instrument by using THG (355 nm) of Nd: YAG laser, Minilite I (Continuum, CA, USA) as excitation source. The signals were monitored with an R2949 photomultiplier. Data were analyzed using the nonlinear least-squares procedure.

Dynamic Light-Scattering (DLS) Studies. Measurements of the size in diameter of Ir complexes were measured at 37 °C using a Zetasizer Nano ZS (Malvern Instruments) spectrometer. The instrument was equipped with a 4 mW He−Ne laser operating at 623 nm, and the sample solutions were filtered through a 0.5 μm filter, they were placed in disposable plastic cuvettes (ZEN0040).

Cell Culture. Jurkat and Molt-4 cell lines were cultured in RPMI 1640 medium supplemented with 10% heat-inactivated fetal calf serum (FCS), L-glutamine, HEPES (2-[4-(2-hydroxyethyl)-1-piperazinyl]ethanesulfonic acid, pK_a = 7.5), penicillin/streptomycin, and monothioglycerol (MTG) in a humidified 5% CO_2 incubator at 37 °C. HeLa-S3 cells, which were provided by Dr. Tomoko Okada (National Institute of Advanced Industrial Science and Technology), were grown in MEM supplemented with 10% FCS L-glutamine, and penicillin/streptomycin under 5% CO_2 at 37 °C. A549 cells were grown in D-MEM (low glucose) supplemented with 10% FCS, L-glutamine, and penicillin/streptomycin under 5% CO_2 at 37 °C.

MTT Assay.[59] Jurkat cells and Molt-4 cells (1.0 × 10^5 cells/mL) were incubated in 10% FCS RPMI 1640 medium containing solution of Ir complexes (0−50 μM), **10a** and **10b** (0−50 μM) under 5% CO_2 at 37 °C for 16 h on 96 well plates (BD Falcon), 0.5% MTT (3-(4,5-dimethyl-2-thiazolyl)-

DOI: 10.1021/acs.bioconjchem.5b00095
Bioconjugate Chem. 2015, 26, 857−879

2,5-diphenyl-2*H*-tetrazolium bromide) reagent in PBS (10 μL) was then added to the cells. After incubation at 37 °C for 4 h, a formazan lysis solution (10% SDS in 0.01 N HCl) (100 μL) was added and the resulting solution incubated for overnight under the same conditions, followed by measurement of absorbance at 570 nm with a microplate reader (BIO-RAD).

After HeLa-S3 cells and A549 cells in RPMI 1640 medium with 10% FCS (1.0×10^5 cells/mL) were seeded into 96 well plates, and incubated for 24 h, MTT assay of them with Ir complexes **6a** was performed according to the same procedure described above.

MTT Assay in the Presence of Caspase Inhibitor (z-VAD-fmk). Jurkat cells (1.0×10^5 cells/mL) were incubated in 10% FCS RPMI 1640 medium containing a solution of the pan caspase inhibitor (z-VAD-fmk) (15 μM) under 5% CO_2 at 37 °C for 1 h on 96 well plates (BD Falcon). Then, TRAIL (0, 450 ng/mL) and Ir complex **6a** (0, 75 μM) were added. After incubation under 5% CO_2 at 37 °C for 16 h, a formazan lysis solution (10% SDS in 0.01 N HCl) (100 μL) was added and the resulting solution incubated overnight under the same conditions, followed by measurement of absorbance at 570 nm with a microplate reader (BIO-RAD).

MTT Assay in the Presence of Necroptosis Inhibitor (Necrostatin-1) or ROS Scavenger (IM-54 and NAC). Jurkat cells (1.0×10^5 cells/mL) were incubated in 10% FCS RPMI 1640 medium containing necroptosis inhibitor (necrostatin-1) (30 μM) or ROS scavenger (IM-54) (10 μM) for 4 h, or NAC (1 mM) for 1 h under 5% CO_2 at 37 °C on 96 well plates. The Ir complex **6a** (0, 75 μM) was then added and subsequent procedures were the same as that for the MTT assay in the presence of the caspase inhibitor.

Fluorescent Microscopy Studies of Jurkat Cells with Ir Complexes. Jurkat cells (1.0×10^6 cells/mL) were incubated, in the absence or the presence of Ir complexes (50 μM or 75 μM), in RPMI 1640 medium with 10% FCS for 1 h under 5% CO_2 at 37 °C. After incubation, the cells were washed twice with ice-cold PBS with 0.1% NaN_3 and 0.5% FCS, and observed on fluorescent microscopy (Biorevo, BZ-9000, Keyence) by using Greiner CELLview Petri dish (35 × 10 mm).

Fluorescent Microscopy Studies of Jurkat Cells with Ir Complexes in the Presence of Inhibitors. Jurkat cells (1.0×10^6 cells/mL) in RPMI 1640 medium with 10% FCS were pretreated with inhibitors under 5% CO_2 at 37 °C for 30 min and then Ir complexes (50 μM) were added into the cells. After incubation at 37 °C for 1 h, cells were washed twice with ice-cold PBS containing 0.5% FCS and 0.1% NaN_3, and observed by fluorescent microscopy (excitation 377 nm, emission 520 nm, FF01 filter) by using Greiner CELLview Petri dish (35 × 10 mm). An FCS free medium was used for spermidine and both FCS and a glucose free medium was used for oligomycin.

PI Staining Assay. Jurkat cells and normal mouse lymphocytes (3×10^5 cells/mL) obtained from lymph nodes of a Balb/c mouse were incubated with the Ir complex (0, 12.5, 25, 50 μM) in RPMI 1640 medium with 10% FCS at 37 °C for 1 h under 5% CO_2 on 96 well plates. The PI was then added and the suspension was further incubated for 5 min at room temperature in the dark, and then observed by fluorescent microscopy (excitation 540 nm, emission 605 nm, TRITC filter). After HeLa-S3 cells (1.0×10^5 cells/mL) in RPMI 1640 medium with 10% FCS were seeded in to 96 well plates, and incubated for 24 h, cells were treated with **6a**, and stained by PI according to the same procedure described above. Cell viability was evaluated by the number of cells, which were not stained by PI.

Mitochondrial Membrane Potential Measurements. After treatment of Jurkat cells (3.0×10^6 cells/mL) treated with **6a** (0, 6.3, 12.5, 25 μM) in 10% FCS RPMI 1640 medium, TMRM (50 nM) was added and incubated for 10 min at 37 °C. The resulting cells were washed twice with ice-cold PBS containing 0.5% FCS and 0.1% NaN_3, and analyzed by Gallios flow cytometer (Beckman Coulter).

Zeta Potential Measurements of Jurkat Cells. Measurements of the ζ potential of Jurkat cells (3×10^5 cells/mL) were measured at 37 °C using a Zetasizer Nano ZS (Malvern Instruments) spectrometer with a constant voltage of 40 V, according to a previously reported procedure.[3k] Jurkat cells (3×10^5 cells/mL) were washed with PBS (10 mM, pH 7.4) filtered through a membrane filter (0.45 μm). The cellular suspensions with or without Ir complexes were dispensed into the disposal ζ cells with gold electrodes (DTS1070), and the resulting suspension was equilibrated for 10 min at 37 °C and the potential was measured.

Preparation of Giant Liposomes. Giant liposomes were prepared from lecithin from egg yolk (WAKO) according to a literature report.[60] The lipids (1.5 mg) dissolved in $CHCl_3$ (1 mL) were added to the 50 mL round-bottom flask. After the addition of MeOH (0.15 mL), 10 mM HEPES buffer (pH 7.4) (7 mL) was then carefully added along the flask walls. The organic solvent was removed by rotary evaporation with slow rotation under reduced pressure at 40 °C. After evaporation, an aqueous suspension (ca. 6 mL) of giant liposomes was obtained. The resulting solution of the giant liposome (50 μL) was added to the 96 well plate and allowed to stand for 1 h, then observed on fluorescent microscopy (Biorevo, BZ-9000 (Keyence).

Cell Cycle Synchronization.[48] Jurkat cells treated with 1 mM thymidine (to arrest cells in G_1/S phase) or 0.15 μg/mL nocodazole (to arrest cells in G_2/M phase) were incubated in 10% FCS RPMI 1640 medium for 16 h at 37 °C. After removal of medium, the cells were retreated with 1 mM thymidine or 0.15 μg/mL nocodazole for 8 h at 37 °C, and then washed by PBS. Cell cycle analysis was performed on harvested cell pellets treated with 0.2% Triton X-100 in PBS, RNase A (100 μg/mL), then PI (50 μg/mL). The resulting mixture was analyzed by means of a Gallios flow cytometer (Beckman Coulter).

Ca^{2+} Measurement. To measure the cytoplasmic Ca^{2+} concentration, Jurkat cells (1×10^6 cells/mL) were incubated with Rhod-4/AM (5 μM) in Ca free RPMI 1640-based buffer containing 103 mM NaCl, 5.4 mM KCl, 0.41 mM $MgSO_4$, 24 mM $NaHCO_3$, 5.6 mM Na_2HPO_4, 11 mM glucose, 10 mM HEPES-NaOH (pH 7.4) for 30 min at 37 °C, then washed with the same buffer twice, and replaced with RPMI 1640-based buffer containing 0.42 mM $CaCl_2$, 103 mM NaCl, 5.4 mM KCl, 0.41 mM $MgSO_4$, 24 mM $NaHCO_3$, 5.6 mM Na_2HPO_4, 11 mM glucose, 10 mM HEPES-NaOH (pH 7.4). The loaded cells were plated on 96 well plates at 37 °C for 10 min and the change in the fluorescent intensity of Rhod-4 after treatment with Ir complex (50 μM) was then observed by fluorescent microscopy (excitation 540 nm, emission 605 nm, TRITC filter). Fluorescence intensity of Rhod-4 was analyzed by BZ analyzer II (Keyence).

DOI: 10.1021/acs.bioconjchem.5b00095
Bioconjugate Chem. 2015, 26, 857−879

■ ASSOCIATED CONTENT

Supporting Information

Chart S1−S3, Figure S1−S23, Table S1, and Movie S1. Mass spectra (Figure S24−S43), HPLC analyses (Figure S44−S63), ^{1}H NMR spectra (Figure S64−S82) of Ir complexes **4**, **5**, **6a**−**6j**, **7a**, **7b**, **8**, **9** and reference compounds **10a**, **10b**, **11**. This material is available free of charge via the Internet at http://pubs.acs.org.

■ AUTHOR INFORMATION

Corresponding Author

*E-mail: shinaoki@rs.noda.tus.ac.jp.

Notes

The authors declare no competing financial interest.

■ ACKNOWLEDGMENTS

This work was supported by grants-in-aid from the Ministry of Education, Culture, Sports, Science and Technology (MEXT) of Japan (No. 22890200, 24890256, and 26860016 for Y.H., and No. 19659026, 22390005, and 24659085 for S.A.), the Uehara Memorial Foundation for Y.H. and High-Tech Research Center Project for Private Universities (matching fund subsidy from MEXT). We thank Prof. Dr. Takeshi Inukai (Department of Pediatrics, School of Medicine, University of Yamanashi), Prof. Dr. Ko Okumura and Prof. Dr. Hideo Yagita (Department of Immunology, School of Medicine, Juntendo University) for the helpful discussion. We also thank Prof. Dr. Akinori Morita (Department of Radiological Science, Institute of Health Biosciences, University of Tokushima) for providing Bcl-2 overexpressed Molt-4 cells and wild-type Molt-4 cells and useful suggestion. We thank Dr. Yuuki Obata (Research Institute for Biomedical Sciences, Tokyo University of Science) for providing filipin, cytochalasin D and useful discussion. We thank Dr. Mitsutoshi Tsukimoto (Faculty of Pharmaceutical Sciences, Tokyo University of Science) for providing A549 cells, RPMI 1640-based buffer, and useful suggestion. We appreciate the aid of Mrs. Fukiko Hasegawa (Faculty of Pharmaceutical Sciences, Tokyo University of Science) for measurement of mass spectra.

■ REFERENCES

(1) (a) Lv, H., Zhang, S., Wang, B., Cui, S., and Yan, J. (2006) Toxicity of cationic lipids and cationic polymers in gene delivery. *J. Controlled Release 114*, 100−109. (b) Madani, F., Lindberg, S., Langel, Ü, Futaki, S., and Gräslund, A. (2011) Mechanisms of cellular uptake of cell-penetrating peptides. *J. Biophys. 2011*, 1−10. (c) Zhi, D., Zhang, S., Cui, S., Zhao, Y., Wang, Y., and Zhao, D. (2013) The headgroup evolution of cationic lipids for gene delivery. *Bioconjugate Chem. 24*, 487−519. (d) Nakase, I., Tanaka, G., and Futaki, S. (2013) Cell-penetrating peptides (CPPs) as a vector for the delivery of siRNAs into cells. *Mol. BioSyst. 9*, 855−861.

(2) (a) Liu, Z., Young, A. W., Hu, P., Rice, A. J., Zhou, C., Zhang, Y., and Kallenbach, N. R. (2007) Tuning the membrane selectivity of antimicrobial peptides by using multivalent design. *ChemBioChem 8*, 2063−2065. (b) Liu, L., Xu, K., Wang, H., Tan, P. K., Fan, W., Venkatraman, S. S., Li, L., and Yang, Y.-Y. (2009) Self-assembled cationic peptide nanoparticles as an efficient antimicrobial agent. *Nat. Nanotechnol. 4*, 457−463. (c) Findlay, B., Zhanel, G. G., and Schweizer, F. (2010) Cationic amphiphiles, a new generation of antimicrobials inspired by the natural antimicrobial peptide scaffold. *Antimicrob. Agents Chemother. 54*, 4049−4058. (d) Chen, C., Pan, F., Zhang, S., Hu, J., Cao, M., Wang, J., Xu, H., Zhao, X., and Lu, R. (2010) Antibacterial activities of short designer peptides: a link between propensity for nanostructuring and capacity for membrane destabilization. *Biomacromolecules 11*, 402−411. (e) Yin, L. M., Edwards, M. A., Li, J., Yip, C. M., and Deber, C. M. (2012) Roles of hydrophobicity and charge distribution of cationic antimicrobial peptides in peptide-membrane interactions. *J. Biol. Chem. 287*, 7738−7745. (f) Wang, G. (2014) Human antimicrobial peptides and proteins. *Pharmaceuticals 7*, 545−594.

(3) (a) Marquez, M., Nilsson, S., Lennartsson, L., Liu, Z., Tammela, T., Raitanen, M., and Holmberg, A. R. (2004) Charge-dependent targeting: results in six tumor cell lines. *Anticancer Res. 24*, 1347−1351. (b) Schröder-Borm, H., Bakalova, R., and Andrä, J. (2005) The NK-lysin derived peptide NK-2 preferentially kills cancer cells with increased surface levels of negatively charged phosphatidylserine. *FEBS Lett. 579*, 6128−6134. (c) Shai, Y., and Papo, N. (2005) Host defense peptides as new weapons in cancer treatment. *Cell. Mol. Life Sci. 62*, 784−790. (d) Hoskin, D. W., and Ramamoorthy, A. (2008) Studies on anticancer activities of antimicrobial peptides. *Biochim. Biophys. Acta 1778*, 357−375. (e) Schweizer, F. (2009) Cationic amphiphilic peptides with cancer-selective toxicity. *Eur. J. Pharmacol. 625*, 190−194. (f) Iwasaki, T., Ishibashi, J., Tanaka, H., Sato, M., Asaoka, A., Taylor, D., and Yamakawa, M. (2009) Selective cancer cell cytotoxicity of enantiomeric 9-mer peptides derived from beetle defensins depends on negatively charged phosphatidylserine on the cell surface. *Peptides 30*, 660−668. (g) Standley, S. M., Toft, D. J., Cheng, H., Soukasene, S., Chen, J., Raja, S. M., Band, V., Band, H., Cryns, V. L., and Stupp, S. I. (2010) Induction of cancer cell death by self-assembling nanostructures incorporating a cytotoxic peptide. *Cancer Res. 70*, 3020−3026. (h) Chen, Y. Q., Min, C., Sang, M., Han, Y. Y., Ma, X., Xue, X. Q., and Zhang, S. Q. (2010) A cationic amphiphilic peptide ABP-CM4 exhibits selective cytotoxicity against leukemia cells. *Peptides 31*, 1504−1510. (i) Riedl, S., Zweytick, D., and Lohner, K. (2011) Membrane-active host defense peptides−challenges and perspectives for the development of novel anticancer drugs. *Chem. Phys. Lipids 164*, 766−781. (j) Sinthuvanich, C., Veiga, A. S., Gupta, K., Gasper, D., Blumenthal, R., and Schneider, J. P. (2012) Anticancer β-hairpin peptides: membrane-induced folding triggers activity. *J. Am. Chem. Soc. 134*, 6210−6217. (k) Gasper, D., Veiga, A. S., Sinthuvanich, C., Schneider, J. P., and Castanho, M. A. R. B. (2012) Anticancer peptide SVS-1: efficacy precedes membrane neutralization. *Biochemistry 51*, 6263−6265. (l) Gaspar, D., Veiga, A. S., and Castanho, A. R. B. (2013) From antimicrobial to anticancer peptides. A review. *Front. Microbiol. 4*, 294. (m) Harris, F., Dennison, S. R., Singh, J., and Phoenix, D. A. (2013) On the selectivity and efficacy of defense peptides with respect to cancer cells. *Med. Res. Rev. 33*, 190−234.

(4) (a) Zachowski, A. (1993) Phospholipids in animal eukaryotic membranes: transverse asymmetry and movement. *Biochem. J. 294*, 1−14. (b) Utsugi, T., Schroit, A. J., Connor, J., Buccana, C. D., and Fidler, I. J. (1991) Elevated expression of phosphatidylserine in the outer leaflet of human tumor cells and recognition by activated human blood monocytes. *Cancer Res. 51*, 3062−3066. (c) Riedl, S., Rinner, B., Asslaber, M., Schaider, H., Walzer, S., Novsk, A., Lohner, K., and Zweytick, D. (2011) In search of a novel target−phosphatidylserine exposed by non-apoptotic tumor cells and metastases of malignancies with poor treatment efficacy. *Biochim. Biophys. Acta 1808*, 2638−2645.

(5) Newcomb, C. J., Sur, S., Ortony, J. H., Lee, O.-S., Matson, J. B., Boekhoven, J., Yu, J. M., Schatz, G. C., and Stupp, S. I. (2014) Cell death versus cell survival instructed by supramolecular cohesion of nanostructures. *Nat. Commun. 5*, 3321.

(6) (a) Dedeian, K., Djurovich, P. I., Garces, F. O., Carlson, G., and Watts, R. J. (1991) A new synthetic route to the preparation of a series of strong photoreducing agents: *fac*-tris-ortho-metalated complexes of iridium(III) with substituted 2-phenylpyridines. *Inorg. Chem. 30*, 1685−1687. (b) Tamayo, A. B., Alleyne, B. D., Djurovich, P. I., Lamansky, S., Tsyba, I., Ho, N. N., Bau, R., and Thompson, M. E. (2003) Synthesis and characterization of facial and meridional tris-cyclometalated iridium(III) complexes. *J. Am. Chem. Soc. 125*, 7377−7387. (c) Lowry, M. S., and Bernhard, S. (2006) Synthetically tailored excited states: phosphorescent, cyclometalated iridium(III) complexes and their applications. *Chem.—Eur. J. 12*, 7970−7977. (d) Evans, R. C., Douglas, P., and Winscom, C. J. (2006) Coordination complexes

DOI: 10.1021/acs.bioconjchem.5b00095
Bioconjugate Chem. 2015, 26, 857−879

exhibiting room-temperature phosphorescence: evaluation of their suitability as triplet emitters for light-emitting diodes. *Coord. Chem. Rev. 250*, 2093−2126. (e) Flamigni, L., Barbieri, A., Sabatini, C., Ventura, B., and Barigelletti, F. (2007) Photochemistry and photophysics of coordination compounds: iridium. *Top. Curr. Chem. 281*, 143−203. (f) Ulbricht, C., Beyer, B., Friebe, C., Winter, A., and Schubert, U. S. (2009) Recent developments in the application of phosphorescent iridium(III) complex systems. *Adv. Mater. 21*, 4418−4441. (g) Chi, Y., and Chou, P.-T. (2010) Transition-metal phosphors with cyclometalating ligands: fundamentals and applications. *Chem. Soc. Rev. 39*, 638−655. (h) Farinola, G. M., and Ragni, R. (2011) Electroluminescent materials for white organic light emitting diodes. *Chem. Soc. Rev. 40*, 3467−3482.

(7) (a) Ho, M.-L., Hwang, F.-M., Chen, P.-N., Hu, Y.-H., Cheng, Y.-M., Chen, K.-S., Lee, G.-H., Chi, Y., and Chou, P.-T. (2006) Design and synthesis of iridium(III) azacrown complex: application as a highly sensitive metal cation phosphorescence sensor. *Org. Biomol. Chem. 4*, 98−103. (b) Schmittel, M., and Lin, H. (2007) Luminescent iridium phenanthroline crown ether complex for the detection of silver(I) ions in aqueous media. *Inorg. Chem. 46*, 9139−9145. (c) Xiong, L., Zhao, Q., Chen, H., Wu, Y., Dong, Z., Zhou, Z., and Li, F. (2010) Phosphorescence imaging of homocysteine and cysteine in living cells based on a cationic iridium(III) complex. *Inorg. Chem. 49*, 6402−6408. (d) Zhao, Q., Li, F., and Huang, C. (2010) Phosphorescent chemosensors based on heavy-metal complexes. *Chem. Soc. Rev. 39*, 3007−3030. (e) Brandel, J., Sairenji, M., Ichikawa, K., and Nabeshima, T. (2010) Remarkable Mg^{2+}-selective emission of an azacrown receptor based on Ir(III) complex. *Chem. Commun. 46*, 3958−3960. (f) Guerchais, V., and Fillaut, J.-L. (2011) Sensory luminescent iridium(III) and platinum(II) complexes for cation recognition. *Coord. Chem. Rev. 255*, 2448−2457. (g) You, Y., Han, Y., Lee, Y.-M., Park, S. Y., Nam, W., and Lippard, S. J. (2011) Phosphorescent sensor for robust quantification of copper(II) ion. *J. Am. Chem. Soc. 133*, 11488−11491. (h) Woo, H., Cho, S., Han, Y., Chae, W.-S., Ahn, D.-R., You, Y., and Nam, W. (2013) Synthetic control over photoinduced electron transfer in phosphorescence zinc sensors. *J. Am. Chem. Soc. 135*, 4771−4787. (i) Ru, J.-X., Guan, L.-P., Tang, X.-L., Dou, W., Yao, X., Chen, W.-M., Liu, Y.-M., Zhang, G.-L., Liu, W.-S., Meng, Y., et al. (2014) Turn-on phosphorescent chemodosimeter for Hg^{2+} based on a cyclometalated Ir(III) complex and its application in time-resolved luminescence assays and live cell imaging. *Inorg. Chem. 53*, 11498−11506.

(8) (a) Wang, X., Jia, J., Huang, Z., Zhou, M., and Fei, H. (2011) Luminescent peptide labeling based on a histidine-binding iridium(III) complex for cell penetration and intracellular targeting studies. *Chem.—Eur. J. 17*, 8028−8032. (b) Shiu, H.-Y., Chong, H.-C., Leung, Y.-C., Zou, T., and Che, C.-M. (2014) Phosphorescent proteins for bio-imaging and site selective bio-conjugation of peptides and proteins with luminescent cyclometalated iridium(III) complexes. *Chem. Commun. 50*, 4375−4378.

(9) (a) Lo, K. K.-W., Louie, M.-W., and Zhang, K. Y. (2010) Design of luminescent iridium(III) and rhenium(I) polypyridine complexes as *in vitro* and *in vivo* ion, molecular and biological probes. *Coord. Chem. Rev. 254*, 2603−2622. (b) Zhang, K. Y., Li, S. P.-Y., Zhu, N., Or, I. W.-S., Cheung, M. S.-H., Lam, Y.-W., and Lo, K. K.-W. (2010) Structure, photophysical and electrochemical properties, biomolecular interactions, and intracellular uptake of luminescent cyclometalated iridium(III) dipyridoquinoxaline complexes. *Inorg. Chem. 49*, 2530−2540. (c) Leung, S.-K., Kwok, K. Y., Zhang, K. Y., and Lo, K. K.-W. (2010) Design of luminescent biotinylation reagents derived from cyclometalated iridium(III) and rhodium(III) bis(pyridylbenzaldehyde) complexes. *Inorg. Chem. 49*, 4984−4995. (d) Zhang, K. Y., Liu, H.-W., Fong, T. T.-H., Chen, X.-G., and Lo, K. K.-W. (2010) Luminescent dendritic cyclometalated iridium(III) polypyridine complexes: synthesis, emission behavior, and biological properties. *Inorg. Chem. 49*, 5432−5443. (e) Zhao, Q., Yu, M., Shi, L., Liu, S., Li, C., Shi, M., Zhou, Z., Huang, C., and Li, F. (2010) Cationic iridium(III) complexes with tunable emission color as phosphorescent dyes for live cell imaging. *Organometallics 29*, 1085−1091. (f) Zhao, Q., Huang, C., and Li, F. (2011) Phosphorescent heavy-metal complexes for bioimaging. *Chem. Soc. Rev. 40*, 2508−2524. (g) Lo, K. K.-W., Li, S. P.-Y., and Zhang, K. Y. (2011) Development of luminescent iridium(III) polypyridine complexes as chemical and biological probes. *New J. Chem. 35*, 265−287. (h) Li, C., Yu, M., Sun, Y., Wu, Y., Huang, C., and Li, F. (2011) A nonemissive iridium(III) complex that specifically lights-up the nuclei of living cells. *J. Am. Chem. Soc. 133*, 11231−11239. (i) You, Y., Lee, S., Kim, T., Ohkubo, K., Chae, W.-S., Fukuzumi, S., Jhon, G.-J., Nam, W., and Lippard, S. J. (2011) Phosphorescent sensor for biological mobile zinc. *J. Am. Chem. Soc. 133*, 18328−18342. (j) Lee, P.-K., Law, W. H.-T., Liu, H.-W., and Lo, K. K.-W. (2011) Luminescent cyclometalated iridium(III) polypyridine di-2-picolylamine complexes: synthesis, photophysics, electrochemistry, cation binding, cellular internalization, and cytotoxic activity. *Inorg. Chem. 50*, 8570−8579. (k) Wu, Y., Jing, H., Dong, Z., Zhao, Q., Wu, H., and Li, F. (2011) Ratiometric phosphorescence imaging of Hg(II) in living cells based on a neutral iridium(III) complex. *Inorg. Chem. 50*, 7412−7420. (l) Murphy, L., Congreve, A., Palsson, L.-O., and Williams, J. A. G. (2010) The time domain in co-stained cell imaging: time-resolved emission imaging microscopy using a protonatable luminescent iridium complex. *Chem. Commun. 46*, 8743−8745. (m) Baggaley, E., Weinstein, J. A., and Williams, J. A. G. (2012) Lighting the way to see inside the live cell with luminescent transition metal complexes. *Coord. Chem. Rev. 256*, 1762−1785. (n) You, Y. (2013) Phosphorescence bioimaging using cyclometalated Ir(III) complexes. *Curr. Opin. Chem. Biol. 17*, 699−707. (o) Cao, R., Jia, J., Ma, X., Zhou, M., and Fei, H. (2013) Membrane localized iridium(III) complex induces endoplasmic reticulum stress and mitochondria-mediated apoptosis in human cancer cells. *J. Med. Chem. 56*, 3636−3644. (p) Zhou, Y., Jia, J., Li, W., Fei, H., and Zhou, M. (2013) Luminescent biscarbene iridium(III) complexes as living cell imaging reagents. *Chem. Commun. 49*, 3230−3232. (q) Lo, K. K.-W., and Li, S. P.-Y. (2014) Utilization of the photophysical and photochemical properties of phosphorescent transition metal complexes in the development of photofunctional cellular sensors, imaging reagents, and cytotoxic agents. *RSC Adv. 24*, 10560−10585.

(10) (a) Zhang, S., Hosaka, M., Yoshihara, T., Negishi, K., Iida, Y., Tobita, S., and Takeuchi, T. (2010) Phosphorescent light-emitting iridium complexes serve as a hypoxia-sensing probe for tumor imaging in living animals. *Cancer Res. 70*, 4490−4498. (b) Yoshihara, T., Kobayashi, A., Oda, S., Hosaka, M., Takeuchi, T., and Tobita, S. (2012) Iridium complex probes for monitoring of cellular oxygen levels and imaging of hypoxic tissues. *Proc. SPIE 8233*, 82330A1−82330A8.

(11) (a) Liu, Z., Salassa, L., Habtemariam, A., Pizarro, A. M., Clarkson, G. J., and Sadler, P. J. (2011) Contrasting reactivity and cancer cell cytotoxicity of isoelectronic organometallic iridium(III) complexes. *Inorg. Chem. 50*, 5777−5783. (b) Liu, Z., and Sadler, P. J. (2014) Organoiridium complexes: anticancer agents and catalysts. *Acc. Chem. Res. 47*, 1174−1185.

(12) (a) Kuil, J., Steunenberg, P., Chin, P. T. K., Oldenburg, J., Jalink, K., Velders, A. H., and Van Leeuwen, F. W. B. (2011) Peptide-functionalized luminescent iridium complexes for lifetime imaging of CXCR4 expression. *ChemBioChem 12*, 1897−1903. (b) Koren, K., Dmitriev, R. I., Borisov, S. M., Papkovsky, D. B., and Klimant, I. (2012) Complexes of Ir^{III}-octaethylporphyrin with peptides as probes for sensing cellular O_2. *ChemBioChem 13*, 1184−1190. (c) Yoshihara, T., Yamaguchi, Y., Hosaka, M., Takeuchi, T., and Tobita, S. (2012) Ratiometric molecular sensor for monitoring oxygen levels in living cells. *Angew. Chem., Int. Ed. 51*, 4148−4151. (d) Dolan, C., Moriarty, R. D., Lestini, E., Devocelle, M., Forster, R. J., and Keyes, T. E. (2013) Cell uptake and cytotoxicity of a novel cyclometalated iridium(III) complex and its octaarginine peptide conjugate. *J. Inorg. Biochem. 119*, 65−74.

(13) Fei and co-workers recently reported on the cationic peptide conjugated heteroleptic cyclometalated Ir complexes having cancer-cell selective cytotoxicity. See: Ma, X., Jia, J., Cao, R., Wang, X., and Fei, H. (2014) Histidine-iridium(III) coordination-based peptide luminogenic cyclization and cyclo-RGD peptides for cancer-cell targeting. *J. Am. Chem. Soc. 136*, 17734−17737.

DOI: 10.1021/acs.bioconjchem.5b00095
Bioconjugate Chem. 2015, 26, 857−879

(14) (a) Aoki, S., Matsuo, Y., Ogura, S., Ohwada, H., Hisamatsu, Y., Moromizato, S., Shiro, M., and Kitamura, M. (2011) Regioselective aromatic substitution reactions of cyclometalated Ir(III) complexes: Synthesis and photochemical properties of substituted Ir(III) complexes that exhibit blue, green, and red color luminescence emission. *Inorg. Chem. 50*, 806−818. (b) Hisamatsu, Y., and Aoki, S. (2011) Design and synthesis of blue-emitting cyclometalated iridium(III) complexes based on regioselective functionalization. *Eur. J. Inorg. Chem.*, 5360−5369. (c) Moromizato, S., Hisamatsu, Y., Suzuki, T., Matsuo, Y., Abe, R., and Aoki, S. (2012) Design and synthesis of a luminescent cyclometalated iridium(III) complex having *N*,*N*-diethylamino group that stains acidic intracellular organelles and induces cell death by photoirradiation. *Inorg. Chem. 51*, 12697−12706. (d) Nakagawa, A., Hisamatsu, Y., Moromizato, S., Kohno, M., and Aoki, S. (2014) Synthesis and photochemical properties of pH responsive tris-cyclometalated iridium(III) complexes that contain a pyridine ring on the 2-phenylpyridine ligand. *Inorg. Chem. 53*, 409−422. (e) Kando, A., Hisamatsu, Y., Ohwada, H., Moromizato, S., Kohno, M., Aoki, S. *Inorg. Chem.* Accepted.

(15) Cantekin, S., de Greef, T. F. A., and Palmans, A. R. A. (2012) Benzene-1,3,5-tricarboxamide: a versatile ordering moiety for supramolecular chemistry. *Chem. Soc. Rev. 41*, 6125−6137.

(16) Lott, R. S., Chauhan, V. S., and Stammer, C. H. (1979) Trimethylsilyl iodide as a peptide deblocking agent. *J. Chem. Soc., Chem. Commun. 11*, 493−495.

(17) We measured UV/vis absorption spectra of all the Ir complexes synthesized in this work in DMSO and confirmed that almost all compounds have similar UV/vis absorption spectra. As examples, those of **5**, **6a**, **7a**, **8**, and **9** are added in Figure S1 in Supporting Information, based on which the concentrations of the Ir complexes were determined. The decrease of the absorbance at ca. 280 nm of Ir complexes **8** and **9** (10 μM) having longer alkyl chains (C12 and C16) is observed in aqueous solution. These data strongly imply that smaller absorption at ca. 280 nm and weaker emission at ca. 500 nm of **8** and **9** than other complexes are caused by the physical properties of these two Ir complexes. We assume that **8** and **9** tend to form some sort of particles, as indicated in Figure S2 in Supporting Information (ref 18).

(18) Mean particle sizes of **8** and **9** (50 μM) in aqueous solution were determined to be ca. 6 nm and ca. 10 nm by means of dynamic light-scattering (DLS) measurement (Figure S2 in Supporting Information). Consideration of these facts with molecular model study of **8** and **9** suggest that these two complexes should have a diameter of 6−8 nm, and that they exist as a monomer and/or in a very small-size assembly to cause decrease in Φ.

(19) The emission spectrum of the dead cells collected after the treatment with **6a** is identical to that of **6a** (Figure S3 in Supporting Information), indicating that strong green emission of the dead cells comes from **6a**, not autofluorescence. The experimental procedure is as follows. Jurkat cells (1×10^5 cells/mL) were incubated in 10% FCS RPMI 1640 medium with **6a** (50 μM) at 37 °C for 1 h, and then the cells were carefully washed three times with ice-cold PBS containing 0.1% NaN_3 and 0.5% FCS. The collected cellular suspension was diluted to in PBS (to ca. 7×10^4 cells/mL), and recorded on spectrofluorometer at 25 °C (excitation at 366 nm).

(20) It is reported that FCS concentrations in medium affect the activity of cationic peptides (Kosuge, M., Takeuchi, T., Nakase, I., Jones, A. T., and Futaki, S. (2008) Cellular internalization and distribution of arginine-rich peptides as a function of extracellular peptide concentration, serum, and plasma membrane associated proteoglycans. *Bioconjugate Chem. 19*, 656−664). Cytotoxic activity of **6a** against Jurkat cells is almost identical in 5% and 10% FCS RPMI 1640 medium, indicating that the effect of FCS concentration is negligible (Figure S4 in Supporting Information).

(21) 10% FCS RPMI 1640 medium was used for MTT assay of Molt-4 cells, HeLa-S3 cells and A549 cells.

(22) Ir complex **6a** exhibits considerable cytotoxicity against a variety of leukemia cell lines. Cytotoxic activity of **4** and **6a** against KOPT-K1, Reh, Nalm6, Raji, U266, RPMI8226, K562, KOCL48, and KOPM30 cells was investigated by Alamer blue assay. The cytotoxicity of **4** (75 μM) against all these cell lines was negligible. On the other hand, the cell viability in the presence of **6a** (75 μM) was <30% for KOPT-K1, Nalm6, Raji, U266, RPMI8226, K562, KOCL48, and KOPM30 and 70% for Reh cells (Hisamatsu, Y., Shibuya, A., Inukai, T., Kagami, K., Abe, M., and Aoki, S. unpublished results).

(23) Since normal lymphocyte have no proliferation property, it is difficult to evaluate the cell viability of normal cells by MTT assay, which requires 16 h. That is why we evaluated the cytotoxicity of Ir complex **6a** by staining with PI after incubation with **6a** for 1 h.

(24) (a) Zhang, Y., Yang, M., Portney, N. G., Cui, D., Budak, G., Ozbay, E., Ozkan, M., and Ozkan, C. S. (2008) Zeta potential: a surface electrical characteristic to probe the interaction of nanoparticles with normal and cancer human breast epithelial cells. *Biomed. Microdevices 10*, 321−328. (b) Hondroulis, E., Zhang, R., Zhang, C., Chen, C., Ino, K., Matsue, T., and Li, C.-Z. (2014) Immuno nanoparticles integrated electrical control of targeted cancer cell development using whole cell bioelectronic device. *Theranostics 4*, 919−930. (c) Gaspar, D., Freire, J. M., Pacheco, T. R., Barata, J. T., and Castanho, M. A. R. B. (2015) Apoptotic human neutrophil peptide-1 anti-tumor activity revealed by cellular biomechanics. *Biochim. Biophys. Acta 1853*, 308−316.

(25) Note that the background green emission of **6a** contained in RPMI 1640-based buffer is minimized for clarity by taking photos in shorter exposure time and by using software (BZ analyzer II, Keyence) installed in fluorescent microscopy (Biorevo, BZ-9000, Keyence).

(26) Slee, E. A., Zhu, H., Chow, S. C., MacFarlane, M., Nicholson, D. W., and Cohen, G. M. (1996) Benzyloxycarbonyl-Val-Ala-Asp (OMe) fluoromethylketone (Z-VAD-FMK) inhibits apoptosis by blocking the processing of CPP32. *Biochem. J. 315*, 21−24.

(27) Gonzalvez, F., and Ashkenazi, A. (2010) New insights into apoptosis signaling by Apo2L/TRAIL. *Oncogene 29*, 4752−4765.

(28) Degterev, A., Hitomi, J., Germscheid, M., Ch'en, I. L., Korkina, O., Teng, X., Abbott, D., Cuny, G. D., Yuan, C., Wagner, G., et al. (2008) Identification of RIP1 kinase as a specific cellular target of necrostatins. *Nat. Chem. Biol. 4*, 313−321.

(29) Dodo, K., Katoh, M., Shimizu, T., Takahashi, M., and Sodeoka, M. (2005) Inhibition of hydrogen peroxide-induced necrotic cell death with 3-amino-2-indolylmaleimide derivatives. *Bioorg. Med. Chem. Lett. 15*, 3114−3118.

(30) Morita, A., Zhu, J., Suzuki, N., Enomoto, A., Matsumoto, Y., Tomita, M., Suzuki, T., Ohtomo, K., and Hosoi, Y. (2006) Sodium orthovanadate suppresses DNA damage-induced caspase activation and apoptosis by inactivating p53. *Cell Death Differ. 13*, 499−511.

(31) Cellular uptake studies of cyclometalated Ir(III) complexes in the presence of CCCP as a metabolic inhibitor, see: (a) Lee, P.-K., Liu, H.-W., Yiu, S.-M., Louie, M. M.-W., and Lo, K. K.-W. (2011) Luminescent cyclometallated iridium(III) bis(quinolylbenzaldehyde) diimine complexes–synthesis, photophysics, electrochemistry, protein cross-linking properties, cytotoxicity and cellular uptake. *Dalton Trans. 40*, 2180−2189. (b) Li, S. P.-Y., Tang, T. S.-M., Yiu, K. S.-M., and Lo, K. K.-W. (2012) Cyclometalated iridium(III)-polyamine complexes with intense and long-lived multicolor phosphorescence: synthesis, crystal structure, photophysical behavior, cellular uptake, and transfection properties. *Chem.—Eur. J. 18*, 13342−13354.

(32) (a) Nabi, I. R., and Le, P. U. (2003) Caveolae/raft-dependent endocytosis. *J. Cell Biol. 161*, 673−677. (b) Khalil, I. A., Kogure, K., Futaki, S., and Harashima, H. (2006) High density of octaarginine stimulates macropinocytosis leading to efficient intracellular trafficking for gene expression. *J. Biol. Chem. 281*, 3544−3551.

(33) Sun, V. Z., Li, Z., Deming, T. J., and Kamei, D. T. (2011) Intracellular fates of cell-penetrating block copolypeptide vesicles. *Biomacromolecules 12*, 10−13.

(34) Seglen, P. O., and Gordon, P. B. (1982) 3-Methyladenine: specific inhibitor of autophagic/lysosomal protein degradation in isolated rat hepatocytes. *Proc. Natl. Acad. Sci. U.S.A. 79*, 1889−1892.

(35) Kimura, T., Takabatake, Y., Takahashi, T., and Isaka, Y. (2013) Chloroquine in cancer therapy: A double-edged sword of autophagy. *Cancer Res. 73*, 3−7.

DOI: 10.1021/acs.bioconjchem.5b00095
Bioconjugate Chem. 2015, 26, 857−879

(36) Dröse, S., and Altendorf, K. (1997) Bafilomycins and concanamycins as inhibitors of V-ATPases and P-ATPases. *J. Exp. Biol. 200*, 1−8.
(37) Novohradsky, V., Liu, Z., Vojtiskova, M., Sadler, P. J., Brabec, V., and Kasparkova, J. (2014) Mechanism of cellular accumulation of an iridium(III) pentamethylcyclopentadienyl anticancer complex containing a *C,N*-chelating ligand. *Metallomics 6*, 682−690.
(38) (a) Cantley, L. C., Jr., Cantley, L. G., and Josephson, L. (1978) A characterization of vanadate interactions with the (Na, K)-ATPase. Mechanistic and regulatory implications. *J. Biol. Chem. 253*, 7361−7368. (b) Karlish, S. J. D., Beauge, L. A., and Glynn, I. M. (1979) Vanadate inhibits (Na^+ + K^+)ATPase by blocking a conformational change of the unphosphorylated form. *Nature 282*, 333−335. (c) Lau, J. S.-Y., Lee, P.-K., Tsang, K. H.-T., Ng, C. H.-C., Lam, Y.-W., Cheng, S.-H., and Lo, K. K.-W. (2009) Luminescent cyclometalated iridium(III) polypyridine indole complexes—synthesis, photophysics, electrochemistry, protein-binding properties, cytotoxicity, and cellular uptake. *Inorg. Chem. 48*, 708−718.
(39) (a) Kakinuma, Y., Hoshino, K., and Igarashi, K. (1988) Characterization of the inducible polyamine transporter in bovine lymphocytes. *Eur. J. Biochem. 176*, 409−414. (b) Cullis, P. M., Green, R. E., Merson-Davies, L., and Travis, N. (1999) Probing the mechanism of transport and compartmentalisation of polyamines in mammalian cells. *Chem. Biol. 6*, 717−729. (c) Sakata, K., Kashiwagi, K., and Igarashi, K. (2000) Properties of a polyamine transporter regulated by antizyme. *Biochem. J. 347*, 297−303. (d) Gardner, R. A., Delcros, J.-G., Konate, F., Breitbeil, F., III, Martin, B., Sigman, M., Huang, M., and Phanstiel, O., IV (2004) N^1-substituent effects in the selective delivery of polyamine conjugates into cells containing active polyamine transporters. *J. Med. Chem. 47*, 6055−6069. (e) Phanstiel, O., IV, Kaur, N., and Delcros, J.-G. (2007) Structure-activity investigations of polyamine-anthracene conjugates and their uptake via the polyamine transporter. *Amino Acids 33*, 305−313. (f) Simoni, E., Bergamini, C., Fato, R., Tarozzi, A., Bains, S., Motterlini, R., Cavalli, A., Bolognesi, M. L., Minarini, A., Hrelia, P., et al. (2010) Polyamine conjugation of curcumin analogues toward the discovery of mitochondria-directed neuroprotective agents. *J. Med. Chem. 53*, 7264−7268. (g) Minois, N., Carmona-Gutierrez, D., and Madeo, F. (2011) Polyamines in aging and disease. *Aging 3*, 716−732. (h) Muth, A., Kamel, J., Kaur, N., Shicora, A. C., Ayene, I. S., Gilmour, S. K., and Phanstiel, O., IV (2013) Development of polyamine transport ligands with improved metabolic stability and selectivity against specific human cancers. *J. Med. Chem. 56*, 5819−5828.
(40) Weak emission of **6a** was observed on the cell membrane of CCCP-treated cells, indicating interaction with the cell membrane (data not shown).
(41) (a) Catterall, W. A., and Striessnig, J. (1992) Receptor sites for Ca^{2+} channel antagonists. *Trends Pharmacol. Sci. 13*, 256−262. (b) Hockerman, G. H., Peterson, B. Z., Johnson, B. D., and Catterall, W. A. (1997) Molecular determinants of drug binding and action on L-type calcium channels. *Annu. Rev. Pharmacol. Toxicol. 37*, 361−396. (c) Triggle, D. J. (2007) Calcium channel antagonists: clinical uses—past, present and future. *Biochem. Pharmacol. 74*, 1−9.
(42) (a) Motulsky, H. J., Maisel, A. S., Snavely, M. D., and Insel, P. A. (1984) Quinidine is a competitive antagonist at alpha 1- and alpha 2-adrenergic receptors. *Circ. Res. 55*, 376−381. (b) Shibata, k., Hirasawa, A., Foglar, R., Ogawa, S., and Tsujimoto, G. (1998) Effects of quinidine and verapamil on human cardiovascular α1-adrenoceptors. *Circulation 97*, 1227−1230.
(43) Schreiber, G., Barak, A., and Sokolovsky, M. (1985) Disopyramide and quinidine bind with inverse selectivity to muscarinic receptors in cardiac and extracardiac rat tissues. *J. Cardiovasc. Pharmacol. 7*, 390−393.
(44) (a) Harrow, J. A., and Dhalla, N. S. (1976) Effects of quinidine on calcium transport activities of the rabbit heart mitochondria and sarcotubular vesicles. *Biochem. Pharmacol. 25*, 897−902. (b) Van Driessche, W. (1984) Physiological role of apical potassium ion channels in frog skin. *J. Physiol. 356*, 79−95. (c) Gunter, T. E., and Sheu, S.-S. (2009) Characteristics and possible functions of mitochondrial Ca^{2+} transport mechanisms. *Biochim. Biophys. Acta 1787*, 1291−1308.
(45) (a) Babcock, D. F., Herrington, J., Goodwin, P. C., Park, Y. B., and Hille, B. (1997) Mitochondrial participation in the intracellular Ca^{2+} network. *J. Cell Biol. 136*, 833−844. (b) Bernardi, P. (1999) Mitochondrial transport of cations: channels, exchangers, and permeability transition. *Physiol. Rev. 79*, 1127−1155. (c) González, A., Schulz, I., and Schmid, A. (2000) Agonist-evoked mitochondrial Ca^{2+} signals in mouse pancreatic acinar cells. *J. Biol. Chem. 275*, 38680−38686. (d) Jambrina, E., Alonso, R., Alcalde, M., del Carmen Rodríguez, M., Serrano, A., Martínez-A, C., García-Sancho, J., and Izquierdo, M. (2003) Calcium influx through receptor-operated channel induces mitochondria-triggered paraptotic cell death. *J. Biol. Chem. 278*, 14134−14145.
(46) Co-staining study of **6a** with a mitochondrial dye (MitoTracker) against Jurkat cells were unsuccessful due to the negligible emission of MitoTracker in dead cells (data not shown).
(47) Floryk, D., and Houštěk, J. (1999) Tetramethyl rhodamine methyl ester (TMRM) is suitable for cytofluorometric measurements of mitochondrial membrane potential in cells treated with digitonin. *Biosci. Rep. 19*, 27−34.
(48) Miyoshi, N., Uchida, K., Osawa, T., and Nakamura, Y. (2004) A link between benzyl isothiocyanate-induced cell cycle arrest and apoptosis: involvement of mitogen-activated protein kinases in the Bcl-2 phosphorylation. *Cancer Res. 64*, 2134−2142.
(49) (a) Kass, G. E. N., and Orrenius, S. (1999) Calcium signaling and cytotoxicity. *Environ. Health Perspect. 107*, 25−35. (b) Orrenius, S., Zhivotovsky, B., and Nicotera, P. (2003) Regulation of cell death: the calcium−apoptosis link. *Nat. Rev. Mol. Cell Biol. 4*, 552−565. (c) Proskuryakov, S. Y., Konoplyannikov, A. G., and Gabai, V. L. (2003) Necrosis: a specific form of programmed cell death? *Exp. Cell Res. 283*, 1−16. (d) Vanlangenakker, N., Berghe, T. V., Krysko, D. V., Festjens, N., and Vandenabeele, P. (2008) Molecular mechanisms and pathophysiology of necrotic cell death. *Cur. Mol. Med. 8*, 2071−220.
(50) (a) Paredes-Gamero, E. J., Casaes-Rodrigues, R. L., Moura, G. E. D. D., Domingues, T. M., Buri, M. V., Ferreira, V. H. C., Trindade, E. S., Moreno-Ortega, A. J., Cano-Abad, M. F., Nader, H. B., et al. (2012) Cell-permeable gomesin peptide promotes cell death by intracellular Ca^{2+} overload. *Mol. Pharmaceutics 9*, 2686−2697. (b) Paredes-Gamero, E. J., Martins, M. N. C., Cappabianco, F. A. M., Ide, J. S., and Miranda, A. (2012) Characterization of dual effects induced by antimicrobial peptides: regulated cell death or membrane disruption. *Biochim. Biophys. Acta 1820*, 1062−1072.
(51) (a) Duchen, M. R. (2000) Mitochondria and calcium: from cell signaling to cell death. *J. Physiol. 529*, 57−68. (b) Dong, Z., Saikumar, P., Weinberg, J. M., and Venkatachalam, M. A. (2006) Calcium in cell injury and death. *Annu. Rev. Pathol. Mech. Dis. 1*, 405−434. (c) Herzig, S., Maundrell, K., and Martinou, J.-C. (2013) Life without the mitochondrial calcium uniporter. *Nat. Cell Biol. 15*, 1398−1400.
(52) (a) Motulsky, H. J., Snavely, M. D., Hughes, R. J., and Insel, P. A. (1983) Interaction of verapamil and other calcium channel blockers with alpha 1- and alpha 2-adrenergic receptors. *Circ. Res. 52*, 226−231. (b) Feldman, R. D., Park, G. D., and Lai, C.-Y. (1985) The interaction of verapamil and norverapamil with beta-adrenergic receptors. *Circulation 72*, 547−554.
(53) Waelbroeck, M., Robberecht, P., De Neef, P., and Cristophe, J. (1984) Effects of verapamil on the binding properties of rat heart muscarinic receptors: Evidence for an allosteric site. *Biochim. Biophys. Acta 121*, 340−345.
(54) (a) Affolter, H., Burkard, W. P., and Pletscher, A. (1985) Verapamil, an antagonist at 5-Hydroxytryptamine receptors of human blood platelets. *Eur. J. Pharmacol. 108*, 157−162. (b) Auguet, M., Delaflotte, S., Clostre, F., and DeFeudis, F. V. (1986) Verapamil as an apparent competitive antagonist of the serotonin receptor of rabbit isolated aorta. *Gen. Pharmacol. 17*, 133−135.
(55) Das, J. (2011) Aliphatic diazirines as photoaffinity probes for proteins: recent developments. *Chem. Rev. 111*, 4405−4417.
(56) (a) Jaouen, G. (2006) *Bioorganometallics*, Wiley-VCH, Weinheim. (b) Hartinger, C. G., Metzler-Nolte, N., and Dyson, P. J.

DOI: 10.1021/acs.bioconjchem.5b00095
Bioconjugate Chem. 2015, 26, 857−879

(2012) Challenges and opportunities in the development of organometallic anticancer drugs. *Organometallics 31*, 5677−5685. (c) Monney, A., and Albrecht, M. (2012) Transition metal bioconjugates with an organometallic link between the metal and the biomolecular scaffold. *Coord. Chem. Rev. 257*, 2420−2433. (d) Dörr, M., and Meggers, E. (2014) Metal complexes as structural templates for targeting proteins. *Curr. Opin. Chem. Biol. 19*, 76−81.

(57) Cinelli, M. A., Cordero, B., Dexheimer, T. S., Pommier, Y., and Cushman, M. (2009) Synthesis and biological evaluation of 14-(aminoalkyl-aminomethyl)aromathecins as topoisomerase I inhibitors: Investigating the hypothesis of shared structure−activity relationships. *Bioorg. Med. Chem. 17*, 7145−7155.

(58) (a) Murov, S. L., Carmichael, I., and Hug, G. L. (1992) *Handbook of Photochemistry*, 2nd ed., Wiley-VCH, Weinheim. (b) De Bernardo, S., Weigele, M., Toome, V., Manhart, K., Leimgruber, W., Böhlen, P., Stein, S., and Udenfriend, S. (1974) Studies on the reaction of fluorescamine with primary amines. *Arch. Biochem. Biophys. 163*, 390−399.

(59) Mosmann, T. (1983) Rapid colorimetric assay for cellular growth and survival: application to proliferation and cytotoxicity assays. *J. Immunol. Methods 65*, 55−63.

(60) Moscho, A., Orwar, O., Chiu, D. T., Modi, B. P., and Zare, R. N. (1996) Rapid preparation of giant unilamellar vesicles. *Proc. Natl. Sci. U.S.A. 93*, 11443−11447.

DOI: 10.1021/acs.bioconjchem.5b00095
Bioconjugate Chem. 2015, 26, 857−879